6-6-1962

The Time Required for Nuclear Fission

William Earn Stein

TIME
REQUIRED
FOR NUCLEAR
FISSION

STEIN

THE TIME REQUIRED FOR NUCLEAR FISSION*

By

William E. Stein

A Dissertation

Submitted in Partial Fulfillment of the

Requirements for the Degree of

Doctor of Philosophy in Physics

The University of New Mexico

1962

*Work performed under the auspices of the U.S. Atomic Energy Commission.

WILLIAM EARL STEIN

This dissertation, directed and approved by the candidate's committee, has been accepted by the Graduate Committee of the University of New Mexico in partial fulfillment of the requirements for the degree of

DOCTOR OF PHILOSOPHY

Stuart A. Northrop
DEAN

June 6, 1962
DATE

Committee

C. P. Leavitt
CHAIRMAN

John R. Sneed

Roy Thomas

PREFACE

The research represented by this dissertation was performed under the Graduate Thesis Program of the Los Alamos Scientific Laboratory, Los Alamos, New Mexico. Under this program an agreement is made between the Los Alamos Scientific Laboratory and the University of New Mexico by which a graduate student, after completing his course work and preliminary requirements at the University, may perform the research for his doctoral degree at Los Alamos.

William E. Stein

Los Alamos, New Mexico

May 1962

ACKNOWLEDGMENTS

I would like to express my appreciation to the administration of the Los Alamos Scientific Laboratory and especially to Dr. J. M. B. Kellogg, the leader of the Physics Division, for the opportunity of performing this work under the Graduate Thesis Program.

I am particularly indebted to Dr. C. P. Leavitt who supervised this research work for the University of New Mexico and to Dr. C. W. Zabel for his guidance and encouragement throughout the course of this work. I wish to thank Dr. D. K. Froman for stimulating discussions and Dr. J. H. Manley who first pointed out to me paucity of previous experimental work on this subject.

I am grateful to E. H. Pierce and J. G. Povelites for the preparation of the sources and to Dr. H. T. Motz and the entire staff associated with the operation of the Omega West Reactor for cooperation and assistance during the course of these measurements. For her assistance in the preparation and typing of this dissertation, I am grateful to K. H. Harper.

William E. Stein

May 21, 1962

ABSTRACT

The present work is concerned with the mean lifetime of compound nuclei formed in the fast-neutron-induced-fission process. A new method for the measurement of these lifetimes is proposed. The present method is based on the recoil of the compound nucleus following neutron capture and the secondary electrons emitted by fission fragments.

Previous experimental and theoretical work concerning the secondary electron yields for fission fragments and other charged particles are reviewed. The importance of the higher energy electrons, the so-called delta rays, formed in the primary ionization process is considered. The subsequent secondary ionization produced by these delta rays provides a natural explanation of a previous experimental fact that the number of electrons emitted by a fission fragment is larger when the fragment emerges than when it enters the same surface. This viewpoint is extended to a consideration of the dependence of the electron yield on the depth beneath the surface at which a fission event takes place. On the basis of a qualitative theory, this yield is expected to increase with depth and approach asymptotically a limiting value which corresponds to the case where the fragment emerges from depths larger than the maximum range of the delta rays.

Measurements of this dependence of the yield on the depth were performed with layers of uranium tetrafluoride. In these measurements

the electrons were detected by accelerating and focusing them on a scintillation detector. A measure of the number of electrons emitted by each fragment was obtained from the height of the pulse from this detector. The general dependence predicted by the theory was observed.

These results were used in an attempt to measure the average distance traversed by the recoiling compound nuclei during the time interval between neutron capture and fission. In one arrangement of the apparatus the compound nuclei with a given recoil velocity were expected to move away from the foil surface a distance proportional to their mean lifetime. Later, the arrangement of the apparatus was changed so that the nuclei were expected to move closer to the surface. Measurements of the average electron yield were made in each position. From a comparison of these results and the previously determined dependence of the yield on depth, an estimate of the average recoil distance and, therefore, a measure of the mean lifetime could be obtained.

Target nuclei of uranium-238 and neptunium-237 were used in this experiment. Neutrons with an assumed fission spectrum were obtained from a reactor.

The results of these measurements showed that the mean lifetimes of the compound nuclei of U-239 and Np-238 were, within the sensitivity of the present method, consistent with zero. Upper limits of the lifetimes have been obtained, however, which are considerably lower than those previously obtained. The total mean lifetimes for target nuclei of U-238 and Np-237 were found to be $\tau(\text{U-238}) < 6 \times 10^{-14}$ sec and $\tau(\text{Np-237}) < 4 \times 10^{-14}$ sec. The partial mean lifetimes for fission and neutron emission were determined from the relation $\Gamma = \Gamma_f + \Gamma_n$ and the

previously measured ratio of the fission and neutron emission widths. The partial mean lifetimes are as follows: τ_f(U-238) $< 4 \times 10^{-13}$ sec; τ_n(U-238) $< 7 \times 10^{-14}$ sec; τ_f(Np-237) $< 9 \times 10^{-14}$ sec; and τ_n(Np-237) $< 7 \times 10^{-14}$ sec.

TABLE OF CONTENTS

TABLE OF CONTENTS (continued)

LIST OF TABLES

LIST OF ILLUSTRATIONS

LIST OF ILLUSTRATIONS (continued)

INTRODUCTION

It is generally accepted that nuclear fission proceeds by a two step process.[1] The first step is the formation of a compound nucleus with a finite lifetime, in which the excitation energy is assumed to be shared by the nuclear constituents. The second step requires the transformation of a sufficient part of this excitation energy into potential energy of deformation of the nucleus, which ultimately leads to fission. During the second step, other processes, such as neutron or gamma-ray emission, may compete with fission. For the present work, only the mean lifetimes of the compound nuclei formed during neutron induced fission will be considered. A further distinction between slow and fast neutron induced fission will be made.

For slow neutron induced fission, where the compound nuclei are excited to levels near the fission threshold, the level widths are small in comparison with the level spacing. Cross section measurements in this energy region provide the fission widths, Γ_f, and the photon emission widths, Γ_γ, for each level. The neutron-emission width, Γ_n, is negligible in this case. The fission widths show considerable fluctuation from level to level, whereas the radiative-capture widths are approximately constant. The average fission widths are about 0.1 ev and the radiative-capture widths are one-half to one-fourth as large. It follows, from the uncertainty relation, that the fission lifetime is about 10^{-14} seconds.[2,3]

When compound nuclei are excited to energies which are a few Mev above the fission threshold, the level widths are large compared to the level spacings. It, thus, becomes impossible to measure the widths of individual resonances and one must be content with measurements of the ratio of widths averaged over many levels of the compound nucleus. In this energy region, the neutron emission width, Γ_n, and the fission width, Γ_f, are dominant, whereas the radiative capture width is negligible. Thus, the total width, Γ_T, is approximately equal to the sum of the fission and neutron emission widths. The ratio Γ_f/Γ_T is obtained from direct comparison of the fission and total cross sections. The ratio Γ_f/Γ_n can be determined either from the fission and neutron-emission cross sections or from the value of Γ_f/Γ_T. Since an application of the uncertainty relation to the width ratios yields only relative partial lifetimes, an independent measurement of the total lifetime τ_T, is required in order to obtain the fission lifetime of compound nuclei in the energy region considered here.

Three attempts to measure τ_T directly have been reported in the literature. The first was a measurement by Green and Alvarez.[4] In this experiment natural uranium and a modulated beam of neutrons were used. Observations were made to determine the time delay of the emission of fission fragments, after the neutron irradiation. The time delay was found to be less than 3×10^{-3} seconds. The other two methods depend upon the recoil of the nucleus after being struck by a fast neutron. Feather[5] demonstrated that at least <u>some</u> of the fissions of uranium, which were induced by 14 Mev neutrons, occurred within 5×10^{-13} seconds. This was the estimated time required for the compound nucleus to stop in

solid matter. This experiment provides neither an upper nor lower limit on the lifetime and would be consistent with a wide range of values for τ_T. Wilson[6] carried out an experiment on U^{235} with approximately 12 Mev neutrons which showed that less than 5×10^{-5} of the fissions were delayed by 10^{-8} seconds. A double ionization chamber was used in this experiment. The arrangement was such that, if the compound nucleus traveled for longer than 10^{-8} seconds before undergoing fission, fission fragment pulses would have been recorded in each half of the chamber. Coincidences were measured between the pulses from the two halves of the chamber to reduce the effect of uranium impurities in the walls of the chamber. This measurement provides an upper limit of 10^{-9} sec for the mean lifetime of the compound nucleus of U^{236}. It is interesting to note, that the first two measurements of the fission lifetime were made within a few months after the discovery of fission by Hahn and Strassmann[7] and that in the subsequent period only one other attempt has been made.

The present work is an exposition and an experimental test of a new method of measuring the mean lifetimes of compound nuclei in the energy region where neutron emission competes favorably with fission. This method is based upon the yield of secondary electrons produced by fission fragments emerging from thin layers of material. In particular, it will be shown that the electron yield is a function of the depth, below the surface, at which the fission event takes place. With a suitable experimental arrangement, this relationship between yield and depth can be found and ultimately used to obtain a measure of the distance traversed by the recoiling compound nucleus during the time between neutron

capture and fission.

Chapter I contains a review of the existing experimental and theoretical work which are applicable to this experiment. A simplified explanation of the present method is given in Chapter II and is followed by a description of the apparatus and electronic equipment in Chapter III. The remaining two Chapters give a complete account of this method and the experimental results.

CHAPTER I

PREVIOUS WORK

Experimental

Although the secondary electron emission by protons, alpha particles and other heavy-charged particles has been extensively studied,[8] only a few measurements regarding the electron yield by fission fragments have been reported.[9,10] In each of these measurements, the electrons, emitted by the passage of a fission fragment through a thin foil, were electrostatically accelerated and focused on a scintillation detector. For these measurements, an accelerating voltage of the order of 10 KV was found to be sufficient. After passing through the foil, some of the fragments were stopped in a second scintillation detector. Only the electron pulses which were accompanied by a pulse from the second detector were recorded on a multichannel pulse-height analyzer. The data were presented in the form of distributions of the number of electrons detected for fragments emerging from foils of various materials, where the conversion from pulse height to number of electrons was obtained by measurements of the pulses from the scintillator caused by low-energy electrons. In one of these investigations,[9] the experimental arrangement was changed to detect electrons emitted by fragments entering the foil surface. The electron distributions obtained in either arrangement were approximately symmetric

and could be represented by a Gaussian distribution plus a tail extending in the direction of larger numbers of electrons. The average number of electrons emitted by fragments entering and emerging from the foil will be denoted by N_o and N_e, respectively.

Stein and Leachman[9] found that N_e was approximately equal to 70 electrons for unactivated foils of nickel, copper, silver and gold. In addition, the ratio of N_e to N_o was found to be about 1.7 for the same surface of a nickel foil. A value of about 120 electrons was obtained for N_e by Fraser and Milton[10] with a foil of 8 $\mu gm/cm^2$ of VYNS coated with 8 $\mu gm/cm^2$ of gold.

The main interest in the electrons emitted by fission fragments has been in the development of fast, efficient detectors for use in fission-fragment time-of-flight measurements. Sufficient descriptions of these detectors are contained in the literature and will not be repeated here. Instead, attention will be focused on the inequality of N_e and N_o. An explanation for this inequality will be sought in the existing theories of secondary electron emission by charged particles.

Theoretical

A complete theoretical description of the emission of secondary electrons from solids for impinging charged particles is not available. The present theories, although limited and inapplicable to fission fragments, can, nevertheless, provide some insight into the present problem. Before reviewing these theories, a brief discussion of the presently accepted views on the energy loss of fission fragments will be given. Following this, the theory of secondary electron emission by high-speed ions which was developed by Sternglass will be considered. The approach to

this problem taken by Kapitza from an entirely different point of view also will be noted.

Fission fragments, in their passage through matter, lose energy in the initial part of their range almost entirely by inelastic collisions with the atomic electrons of the stopping material. Although, in reality, there is a continuous transition between one process and the other, the energy of the fragment is assumed to be expended in two distinct types of collision processes. In the first, small amounts of energy are transferred in each collision, whereas in the second, large amounts of energy are transferred to an unbound electron. These two types are generally referred to as distant or resonant and close or free collisions, respectively. The most probable of the ionizing collisions are of the first type in which a relatively slow electron is ejected. The kinetic energy of these electrons is of the order of a few electron volts. Occasionally, an ionizing collision of the second type occurs in which a secondary electron of relatively high energy is produced. The maximum energy for these electrons is given by $4(m_e/M_f)E_f$, where m_e and M_f are the electronic and fragment mass, respectively, and E_f is the fragment energy. For unslowed fission fragments, the maximum energy of these so-called delta rays is approximately 1-2 Kev. Although the number of delta rays is a small fraction of the total number of electrons produced in the primary ionization process, the total energy expended in their production is not negligible. These delta rays are emitted preferentially in the forward direction and expend their energy in secondary ionization processes. The total ionization is given by the sum of the primary and secondary ionizations. Thus, a major portion of

the energy expended by a fission fragment is rapidly converted into the kinetic energy of slow electrons. For a description of the initial spatial distribution of these electrons and for estimates of the number of electrons which escape from the surface of the slowing material, the published theories will now be considered.

Sternglass[11] has presented a theory which considers the production and escape of low-energy secondary electrons produced by high-speed ions. This work deals primarily with the secondary electron yield from a metal surface under bombardment by protons in the Mev energy range, although an extension to heavier particles with lower velocity is indicated. The energetic ions were assumed to be incident normally on a surface and the depth below this surface was represented by x, measured in the direction of the incident particles. The number of low-energy secondary electrons, referred to hereafter as secondaries, originating in unit layer dx at depth x was calculated in two parts, corresponding to those produced by primary ionization, $n_{se}^{(1)}$, and those produced by secondary ionization, $n_{se}^{(2)}$. In terms of the mean energy loss per secondary formed, E_o, and the mean energy loss per unit distance going directly into slow secondary production $\langle dE/dx \rangle^{(1)}$, he obtained the equation

$$n_{se}^{(1)}(v,x) = (1/E_o)\langle dE/dx \rangle^{(1)}, \qquad (1)$$

where v is the velocity of the incident ion. In order to obtain an expression for $n_{se}^{(2)}$, it was necessary to sum over the contributions made by the delta rays formed all along the track of the ion. This led to an expression of the form

$$n_{se}^{(2)}(v,x) = f(v,x)(1/E_o) \langle dE/dx \rangle^{(2)}, \quad (2)$$

where $\langle dE/dx \rangle^{(2)}$ was the mean energy loss per unit path length going into the formation of delta rays. The factor $f(v,x)$ represented the fraction of $\langle dE/dx \rangle^{(2)}$ available for formation of secondaries in the secondary ionization process at depth x. For protons, in the energy region considered here, the theories of Bohr[12] and Bethe[13] have shown that the total energy loss is divided equally between the two types of collision processes, i.e.,

$$\langle dE/dx \rangle^{(1)} = \langle dE/dx \rangle^{(2)} = (1/2) \langle dE/dx \rangle , \quad (3)$$

where $\langle dE/dx \rangle$ is the total energy loss per unit path length. The total number of secondaries, n_{se}, was, therefore, given by

$$n_{se}(v,x) = (1/2\ E_o) \langle dE/dx \rangle [1 + f(v,x)] \quad (4)$$

The probability $P(x)$ for a secondary electron formed at a depth x below the surface to migrate to and escape from the surface was assumed to be

$$P(x) = \omega \exp(-x/L_s) , \quad (5)$$

where ω is a constant approximately equal to 0.5 and L_s is a characteristic length of the order of the distance between inelastic collisions of the secondaries with the electrons of the solid. The yield from a thin layer of width dx, located at depth x, was given by

$$dN = n_{se}(v,x)\ P(x)dx . \quad (6)$$

Substitutions from Equations (4) and (5) and a summation over all layers gave

$$N = \int_o^\infty (1/2\ E_o) \langle dE/dx \rangle [1 + f(v,x)]\ \omega \exp(-x/L_s)dx . \quad (7)$$

The expression derived by Bohr[12] was used for $\langle dE/dx \rangle$ and a value of 25 ev was adopted for E_o.

To determine the factor $f(v,x)$, which represented the contribution of the delta rays to the yield of secondaries, Sternglass proceeded as follows: The average number of slow secondaries formed in a unit layer dx at depth x by fast delta rays originating at depth z was given by

$$dn_{se}^{(2)}(v,x) = (1/E_o)\langle dE/dz \rangle^{(2)} g(x-z,v)dz \ . \qquad (8)$$

In this expression, $g(x-z,v)$ represented the spatial distribution of the energy carried away by the delta rays originating in dz. The total number of secondaries formed at a depth x in this secondary ionization process was given by

$$n_{se}^{(2)}(v,x) = \int_o^\infty (1/E_o)\langle dE/dz \rangle^{(2)} g(x-z,v)dz \ . \qquad (9)$$

In the region of interest, where $\langle dE/dz \rangle^{(2)}$ could be considered constant, this equation reduced to

$$n_{se}^{(2)}(v,x) = f(v,x)(1/E_o)\langle dE/dz \rangle^{(2)} \ , \qquad (10)$$

where

$$f(v,x) = \int_o^\infty g(x-z,v)dz \ . \qquad (11)$$

The exact form of the function $g(x-z,v)$ was not determined. This would have involved a complicated calculation based on transport theory. Instead, Sternglass obtained an approximation to $g(x-z,v)$ based on simple diffusion theory in which the delta rays were considered to diffuse from a plane source located at depth z. In order to account for the initial forward motion of the delta rays, diffusion lengths of different magnitudes were used. The forward and backward diffusion lengths were

designated by L_δ and L_δ', respectively, where L_δ was assumed to be larger than L_δ'. The evaluation of Eq. (11) led to

$$f(v,x) = (1 + L_\delta'/L_\delta)^{-1} \{[1 - \exp(-x/L_\delta)] + L_\delta'/L_\delta\} . \qquad (12)$$

This completes the outline of the theory as presented by Sternglass.

With one minor change, an elementary theory for the production of secondary electrons by fission fragments may be obtained. Bohr[12] has shown that fission fragments lose energy predominantly in free collisions and that Eq. (3) must be replaced by

$$\langle dE/dx\rangle^{(1)} = \kappa \langle dE/dx\rangle , \qquad (13)$$

where κ is approximately 0.15 . Correspondingly, Eq. (4) must be replaced by

$$n_{se}(v,x) = (1/E_o)\langle dE/dx\rangle [\kappa + (1 - \kappa) f(v,x)] , \qquad (14)$$

and Eq. (7) becomes

$$N = \int_o^\infty (1/E_o) \langle dE/dx \rangle [\kappa + (1 - \kappa) f(v,x)] \omega \exp(-x/L_s) dx. \qquad (15)$$

From the point of view of the present work, the most important consequence of this theory is contained in Eq. (14). Even if $\langle dE/dx\rangle$ is constant in the region of interest, the number of secondaries in dx at depth x, $n_{se}(v,x)$, is still a function of x. This can be seen by substituting Eq. (12) into Eq. (14) and rearranging the terms in the square brackets. The result is

$$n_{se}(v,x) = (1/E_o) \langle dE/dx \rangle \{a + b [1 - \exp(-x/L_\delta)]\} , \qquad (16)$$

where

$$a = (\kappa + L_\delta'/L_\delta) (1 + L_\delta'/L_\delta)^{-1}, \; b = (1 - \kappa) (1 + L_\delta'/L_\delta)^{-1} ,$$

and $a + b = 1$.

In many respects this theory is similar to the semiempirical theory of secondary electron emission developed by Salow, Bruning, and others. Each of these theories contains the same oversimplifying assumptions summarized by Dekker.[14] Nevertheless, this theory is believed to provide a qualitative description of the phenomenon of secondary electron emission by fission fragments. It will now be employed to obtain the ratio N_e/N_o for foil conditions similar to those which existed in the experimental work mentioned above.

Consider a fission fragment passing normally through a semi-infinite foil of thickness, L, shown in Fig. 1 . For the purpose of this calculation, the two surfaces will be assumed to have identical characteristics. The thickness, L, is assumed to be large compared to either L_s or L_δ. As an added simplification, the mean energy loss per unit distance, $\langle dE/dx \rangle$, will be considered constant. Under these conditions, the number of secondary electrons emitted as the fission fragment enters the foil is given by

$$N_o = (1/E_o)\langle dE/dx\rangle \int_o^L \{a + b\,[1 - \exp(-x/L_\delta)]\}\ \omega \exp(-x/L_s)\, dx. \quad (17)$$

The integration gives

$$N_o \approx (\omega/E_o)\langle dE/dx \rangle L_s(a + L_s/L_\delta)(1 + L_s/L_\delta)^{-1}, \quad (18)$$

where the approximation is for $L \gg L_s$ and $L \gg L_\delta$. The number of <u>slow</u> electrons emitted by the fragment as it emerges from this foil is given by

$$N_e = (1/E_o)\langle dE/dx\rangle \int_o^L \{a + b\,[1 - \exp(-x/L_\delta)]\}\ \omega \exp[-(L-x)/L_s]dx. \quad (19)$$

Here, the delta rays which escape from the foil are neglected.

Fig. 1.--Electrons emitted from the surfaces of a foil by a fission fragment.

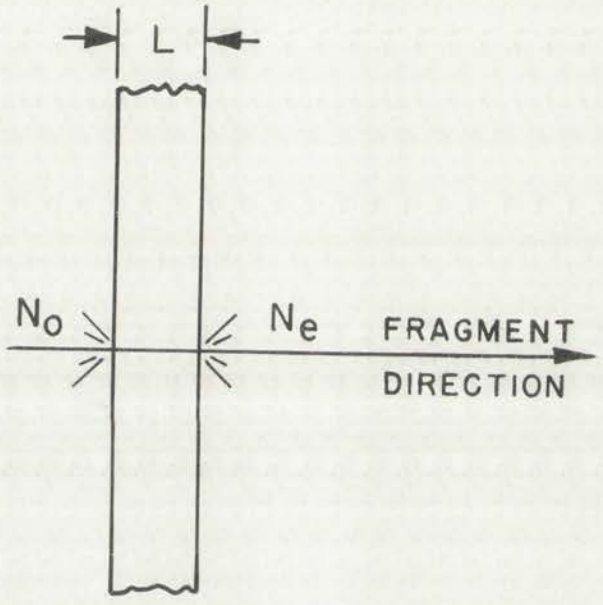
L
No
Ne
FRAGMENT
DIRECTION

With the same approximations and the fact that a + b = 1, the result is

$$N_e \approx (\omega/E_o) \langle dE/dx \rangle L_s . \tag{20}$$

Therefore,

$$N_e/N_o \approx (1 + L_s/L_\delta)(a + L_s/L_\delta)^{-1} . \tag{21}$$

Since the values of κ, L_δ', L_δ and L_s are not known with sufficient accuracy, a numerical estimate of this ratio will not be given. For the present, it will be sufficient to note that, since $a < 1$, the ratio N_e/N_o is greater than unity for all finite values of L_δ. This is consistent with the experimental result. Of equal interest, is the minimum foil thickness, L_m, above which the ratio does not change appreciably. If L_s and L_δ are of comparable magnitude, the ratio is expected to be slowly varying for L_m greater than the range of the most energetic delta ray. For a fission fragment with mass M_f = 100 amu and E_f = 100 Mev, the maximum delta-ray energy is about 2 Kev. According to Feldman,[15] the range in nickel of an electron with this energy is about 300 angstroms. Thus, the ratio N_e/N_o is expected to be practically constant for foil thicknesses greater than a few hundred angstroms.

Another approach to this problem was taken by Kapitza. His theory attempts to explain the secondary electron emission by incident alpha particles. Immediately after the passage of the alpha particle into the solid, the ionized electrons were assumed to be contained in a cylinder of small cross section and to possess a total kinetic energy equal to that lost by the alpha particle. This energy was to have been dissipated along the radius of the cylinder according to the ordinary laws of thermal conductivity. The electrons were then assumed to be

emitted, according to Richardson's law, from the cross section of the cylinder which coincided with the surface of the body. This presentation contained a discussion of the correlation between the angle of emission and the energy of the delta rays, but this angular dependence was not included in the calculation. As a result, the theory does not make a distinction between a particle entering or emerging from the material. The same number of electrons would be predicted in either case. Although this particular inadequacy could be corrected by the proper choice of the initial temperature condition, it is of minor consequence in comparison with the other difficulties of this theory. The main objections are as follows: It is assumed that thermodynamic equilibrium is established in the energy exchange between the alpha particles and the material. The theory leads to a dependence of the yield on the thermal constants and the work function of the material which is in disagreement with experimental measurements.[11]

CHAPTER II

THE PRESENT METHOD

This chapter contains a simplified description of a new method for measuring the mean lifetimes of certain compound nuclei. In order to establish firmly the physical principles involved, only the essential features of this method are presented here. The more complicated aspects will be considered, as they arise, in the development of the later chapters.

The basis of the present method is the dependence of the electron yield on the depth, below a foil surface, at which the fission event takes place. The theory outlined in the previous chapter will be extended to indicate the qualitative features of this function. Next, the recoil of a compound nucleus after neutron capture will be discussed. In particular, the average distance, d, traversed by the compound nucleus during the time interval, τ, between neutron capture and fission will be estimated. Finally, it will be shown that, with a suitable experimental arrangement, measurements of the average electron yield provide an estimate of d and, therefore, of the mean lifetime, τ.

Electron Yield as a Function of Depth

Consider a hypothetical experiment in which a source of fission fragments is positioned at successive depths, x, below the plane surface

of some material as shown in Fig. 2a. The thickness of this material is assumed to be large compared with the range of the most energetic delta ray. In this experiment, only the fission fragments whose directions are parallel to the foil normal will be considered. Let N(x) represent the average electron yield for fragments originating at depth x. The yield for fragments entering the surface will again be represented by N_o. The yield, N_o, applies not only to all source positions outside of the material and to the right of the surface under consideration, but also to the case where x is zero.

According to Eq. (16) of the qualitative theory, the number of secondaries originating in unit layer dy, at depth y, is given by

$$n_1(y) = (1/E_o)\langle dE/dx\rangle \left(a+b \left\{ 1- \exp\left[-(x-y)/L_\delta\right] \right\} \right) \text{ for } 0 \leq y \leq x \qquad (22)$$

and

$$n_2(y) = (1/E_o)\langle dE/dx\rangle \left(a+b \left\{ 1-\exp\left[-(y-x)/L_\delta\right] \right\} \right) \text{ for } y \geq x. \qquad (23)$$

The total number of <u>slow</u> electrons emitted from the surface as a function of source position is

$$N(x) = \int_0^x n_1(y)\, \omega \exp(-y/L_s)\, dy + \int_x^\infty n_2(y)\, \omega \exp(-y/L_s)\, dy \qquad (24)$$

Since it is assumed that the thickness of the material is large compared to L_δ, the error introduced by allowing the upper limit of the second integral to approach infinity is negligible. The integration for a constant $\langle dE/dx\rangle$ gives

$$N(x) = c_1 + c_2 \left[(L_s + L_\delta)\, e^{-x/L_\delta} - 2L_s\, e^{-x/L_s} \right], \qquad (25)$$

where

$$c_1 = (\omega/E_o)\langle dE/dx\rangle (a+b) L_s \text{ and } c_2 = (\omega/E_o)\langle dE/dx\rangle (b\, L_s\, L_\delta)/(L_s^2 - L_\delta^2).$$

Fig. 2.--Electron yield as a function of source position.

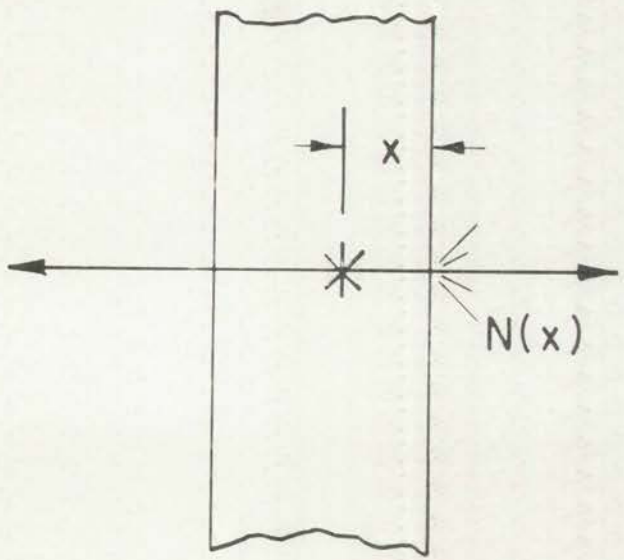

(a)

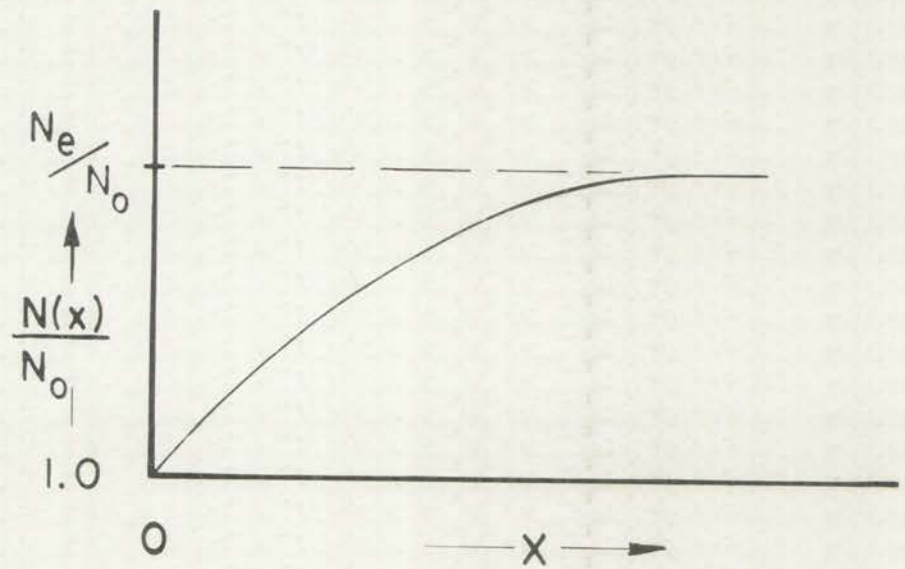

(b)

For $x = 0$, Eq. (25) reduces to $N_o = c_1 + c_2 (L_\delta - L_s)$. (26)

The relative yield is given by

$$N(x)/N_o = c_3 + c_4 [(L_s + L_\delta) \exp(-x/L_\delta) - 2L_s \exp(-x/L_s)], \quad (27)$$

where $c_3 = c_1/[c_1 + c_2 (L_\delta - L_s)]$ and $c_4 = c_2/[c_1 + c_2 (L_\delta - L_s)]$.

The result given in Eq. (27) is based on an approximate theory. Therefore, only the general features of this function will be considered. From the discussion given by Sternglass,[11] it is expected that $L_\delta \approx 4L_s$. With this estimate, the slope is given by

$$d(N/N_o)/dx = [b/(a + 1/4)(3/4)L_\delta][(5/4)\exp(-x/L_\delta) - 2 \exp(-4x/L_\delta)] \quad (28)$$

which is positive for all values of x greater than $0.16L_\delta$. Thus, $N(x)/N_o$ is expected to be unity at x equal to zero and to approach asymptotically the value of N_e/N_o given by Eq. (21) for values of x large compared to the range of the most energetic delta rays. A schematic representation of $N(x)/N_o$ is shown in Fig. 2b. In this illustration, the details of this function for x less than about $0.3 L_\delta$ have been ignored and the curve has been drawn as a monotonically increasing function of x.

Recoil of the Compound Nucleus

In this section, the recoil of a compound nucleus formed by fast-neutron capture is considered. Of particular importance is the recoil

velocity of a fissionable nucleus following the capture of a neutron with a kinetic energy of about 3 Mev. This energy has been chosen as a compromise between two incompatible requirements: (1) The nuclear lifetime is expected to decrease rapidly with increasing excitation of the compound nucleus. It is, therefore, desirable to limit this excitation energy to a value which is one or two Mev above the fission barrier. (2) On the other hand, it is also desirable to form the compound nucleus with as large a recoil velocity as possible. Three Mev also corresponds closely to the average energy of the effective neutrons used in the present work.

Consider a neutron with velocity, $\vec{v}_n$, and mass, μ, incident on a target nucleus of mass, M, at rest. The initial momentum of the system is $\mu \vec{v}_n$. Immediately after neutron capture by the nucleus, the momentum of the system is $(M + \mu) \vec{v}_c$, where $\vec{v}_c$ is the initial velocity of the compound nucleus. From the principle of conservation of momentum, it follows that $\vec{v}_c = \mu \vec{v}_n/(M + \mu)$. In the case of a U-238 target nucleus, for example, the magnitude of the initial recoil velocity is 10^7 cm/sec and the initial energy of the recoil nucleus is 12.5 kev. If collisions between the recoiling nucleus and the atoms of the surrounding material are temporarily neglected, the recoil velocity will be constant. With this assumption, the mean distance traversed by the compound nucleus, d, with speed, v_c, and the mean lifetime, τ, is given by $d = v_c \tau$. From the value of τ mentioned above and the value of v_c from this example, it is expected that $d \approx 10^{-7}$ cm. Conversely, if the values of v_n, μ and M are known, the mean lifetime can be obtained from a measurement of the mean recoil distance. The latter procedure is followed in the present work. The method used to measure this recoil distance is the subject of the next section.

Measurement of the Recoil Distance

In the present experiment the mean recoil distance is determined by measurements of the average electron yield from a thin deposit of fissile material. The relationship between electron yield and recoil distance depends upon the experimental arrangement. In the following example, this relationship will be estimated for conditions similar to those used in the present experiment.

Consider a thin layer of fissile material deposited on one surface of a supporting foil. It is required that this supporting foil (1) be thin compared to the range of a fission fragment, (2) be of sufficient strength to withstand the deposition of the fissile layer by vacuum evaporation, and (3) be a good conductor of electricity. Commercially available nickel foils with a thickness of 0.1 mg/cm^2 were found to be satisfactory for this purpose and were used exclusively in this experiment (see Appendix A). The fissile layers were prepared by vacuum evaporation of either UF_4 or NpF_4. Although this discussion is valid for either compound, the fissile layer, in this example, is assumed to be UF_4 in which the uranium consists entirely of the isotope U-238. Such a foil is shown in Fig. 3, where the thickness of the U-238 layer is designated by L. Here, L is assumed to be smaller than L_m defined above. It is convenient to define the direction of the incident neutrons by the unit vector $\vec{n}$ and the direction of the normal to the fissile layer by the unit vector $\vec{u}$ (not shown). Furthermore, for the purpose of this discussion, it will be assumed that neutrons are captured only by nuclei in the infinitesimal layer at depth L/2. Figure 3c shows schematically the relative electron yield versus the source depth given by Eq. (27) which was

Fig. 3.--Relative yield as a function of average recoil distance.

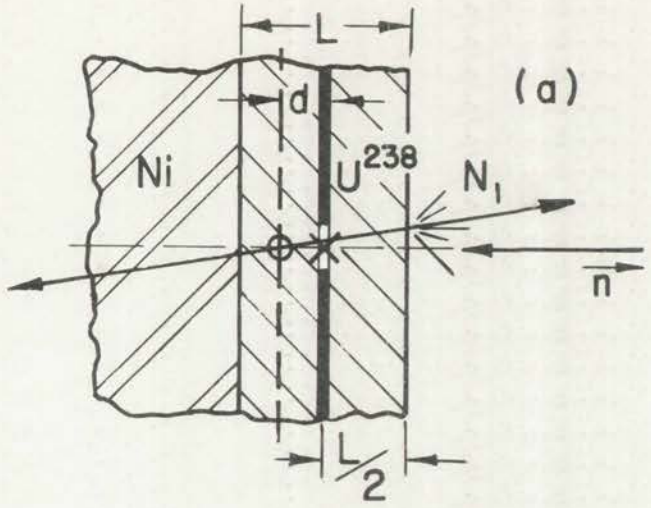

Position 1

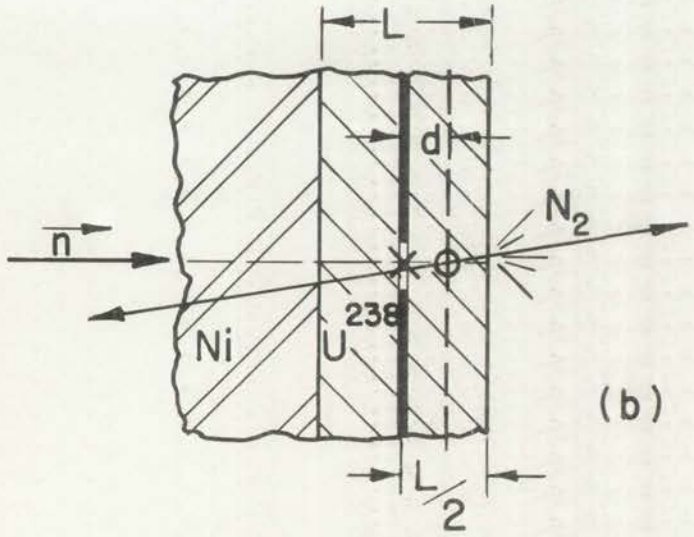

Position 2

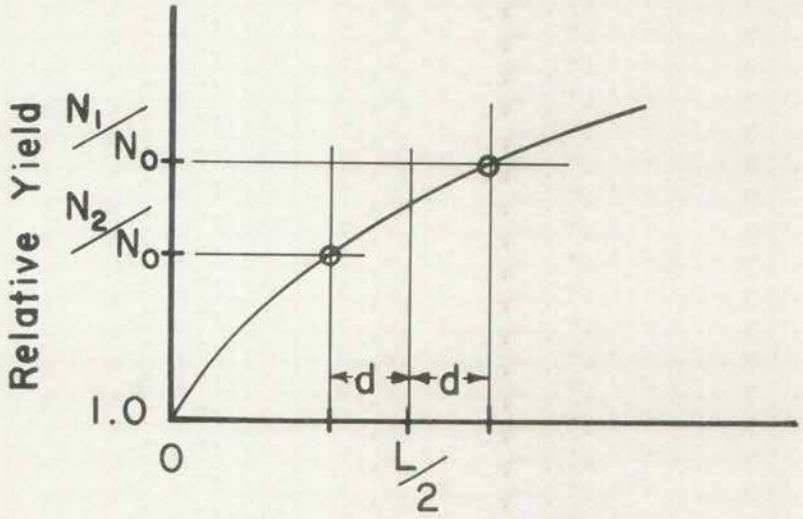

(c)

for fragments emitted parallel to the foil normal. Figure 3a shows the foil in position 1, where $\vec{u} = -\vec{n}$. In this case, the compound nuclei are driven deeper into the foil. The average depth of the source of fission fragments is, therefore, $L/2 + d$. If only those fission events in which the fragments merge within a few degrees with respect to the foil normal are considered, the relative yield will be N_1/N_o as shown in Fig. 3c. In position 2, the neutron beam is in the direction of the normal to the U-238 layer which is represented by $\vec{u} = \vec{n}$ as shown in Fig. 3b. The average depth of the source of fission fragments, in this case, is $L/2 - d$, and the relative yield will be given by N_2/N_o as shown in Fig. 3c. It is evident that N_1/N_o is greater than N_2/N_o for all finite values of d. Furthermore, if the function $N(x)/N_o$, represented by Eq. (27), were known with sufficient accuracy, a value of d could be found from a measurement of N_1/N_2 with a foil of known thickness, L. The above discussion, although greatly oversimplified, presents the basic principles of the present method.

The actual procedure is to sum the contributions to the electron yield from all infinitesimal layers of the uranium deposit. The details of this calculation are given in Chapter V.

The measurements required in this experiment fall in two distinct categories: First, the function $N(x)/N_o$ must be determined experimentally for a UF_4 layer. Second, measurements of the ratio N_1/N_2 must be made with uranium layers of the proper thickness, L. An important consequence of this method is now apparent. In each of these measurements, only a relative yield is required. At no time is it necessary to obtain the yield absolutely; a fact which greatly simplifies the experimental procedure. It is,

therefore, sufficient, for each measurement, merely to determine a quantity which is proportional to the average electron yield. In the present work, the measured quantity was the height of a pulse, which was obtained by accelerating the electrons to a scintillation detector. Since the proportionality factor cancels, the relative pulse height is then equal to the relative yield.

CHAPTER III

APPARATUS AND PROCEDURES

The apparatus used in the present experiment was designed and constructed for the purpose of measuring the relative number of electrons emitted from various foils by fission fragments. In regard to these yield measurements, the present method is similar to those employed in earlier experiments. In those experiments, electrons emitted from thin foils were electrostatically accelerated and focused to a scintillation detector. For a fixed lens voltage, the height of the pulse from the electron detector was assumed to be proportional to the number of electrons emitted by the fission fragment. In most cases, only the electron pulses accompanied by a pulse from an auxiliary fragment detector were recorded.

Vacuum Chamber

In the present experiment, two cylindrical lenses of a type similar to the one discussed by Kleynen[16] were used. These lenses are shown back-to-back in Fig. 4. The lens elements were constructed of 0.064 inch thick brass plates and, where necessary, were provided with screen-covered holes to allow the fission fragments and neutrons to pass through the lens structure. Separation of the plates was by means of 0.936 inch long brass spacers and Teflon insulators. The source from which the electrons were emitted (see Appendix A) is shown mounted on the central element which was common to both lenses. With the central three elements at negative 15 KV

Fig. 4.--Diagram of the electron lens and detector.

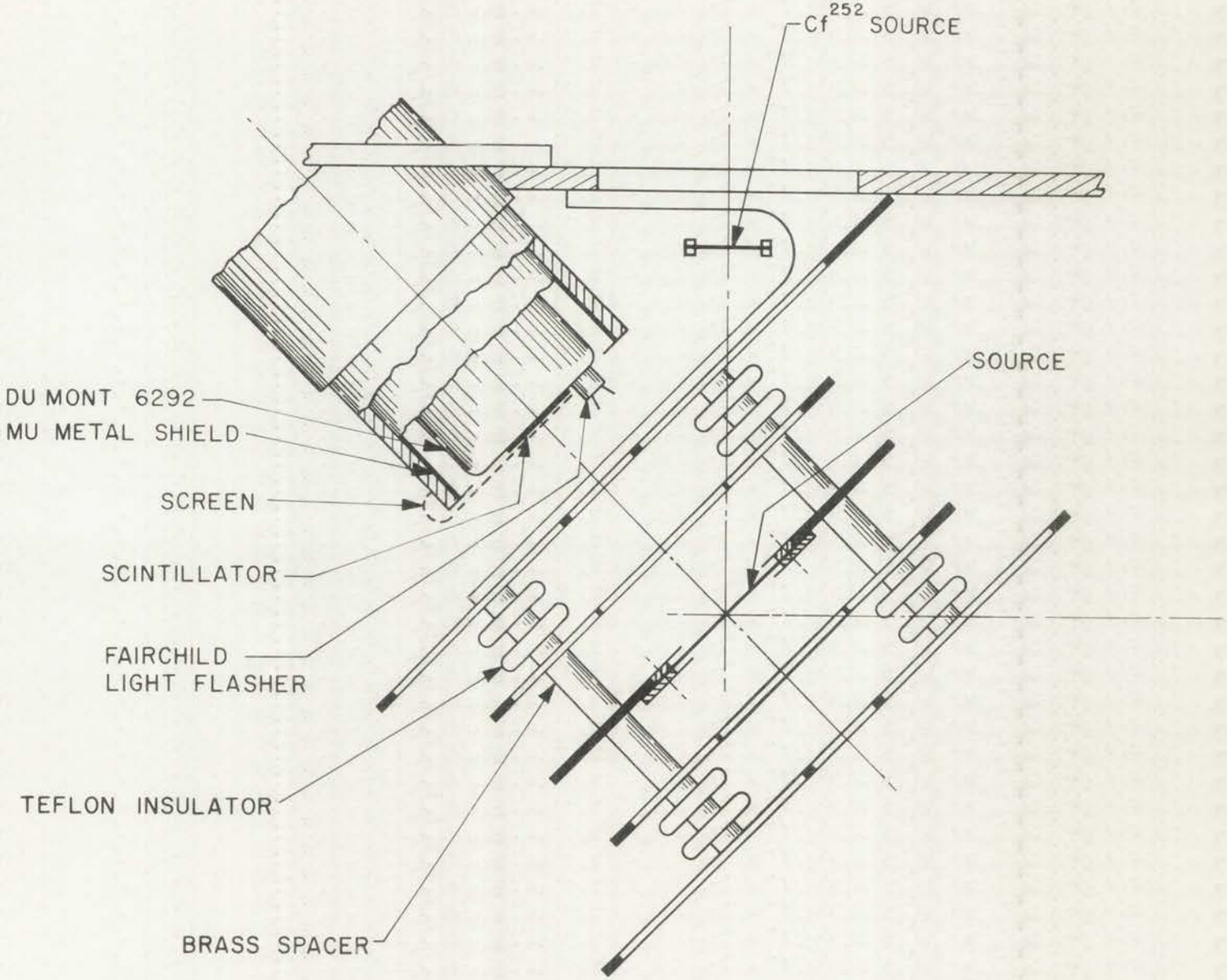
Cf^{252} SOURCE
SOURCE
DU MONT 6292
MU METAL SHIELD
SCREEN
SCINTILLATOR
FAIRCHILD
LIGHT FLASHER
TEFLON INSULATOR
BRASS SPACER

with respect to ground, and the outer two elements grounded, electrons emitted from the top surface of the source were accelerated and focused to the electron detector. Electrons emitted from the bottom surface were likewise focused by the lower lens. However, these electrons were not detected. The purpose of this second lens was merely to provide a well-defined trajectory for these electrons which otherwise could produce spurious pulses in another nearby scintillation detector. The electron detector consisted of a 0.002-inch thick, one-inch diameter plastic scintillator optically coupled to a Type 6292 Du Mont photomultiplier. Magnetic shielding was provided by means of concentric cylinders of Mu metal and mild steel. To reduce the surface charge, a grounded screen with a transmission of 93 percent was mounted in contact with the exposed surface of the scintillator.

The electron detector and lens structure were mounted coaxially on a circular brass plate, hereafter referred to as the turntable. In this arrangement, the angle between the axes of the lens and the turntable was 45 degrees and the point of intersection was at the center of the source. The entire assembly was mounted by means of roller bearings on a stationary circular ring which was located inside the vacuum chamber. This chamber, shown in Fig. 5, was in the form of a vertical-right-circular cylinder with a diameter of 20 inches and a height of 17 inches. Constrained by the roller bearings, the turntable was able to rotate about the vertical axis. An electric motor was provided inside the vacuum chamber for this purpose.

Also shown in Fig. 5, are two fission fragment detectors. Each of these detectors consisted of a 0.002-inch thick, four-inch diameter plastic

Fig. 5.--Cross-section view of the vacuum chamber.

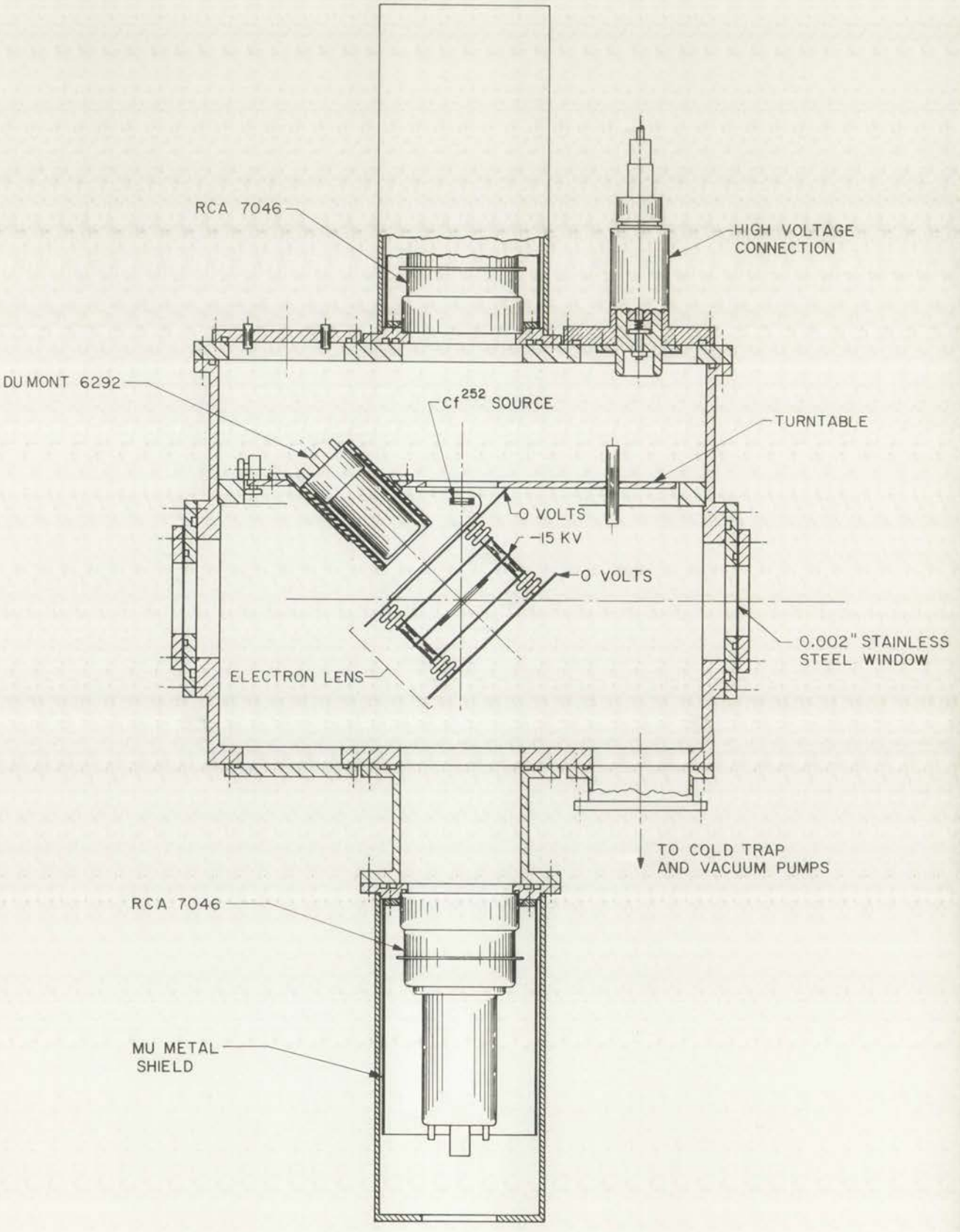
RCA 7046
HIGH VOLTAGE CONNECTION
DU MONT 6292
Cf^{252} SOURCE
TURNTABLE
0 VOLTS
-15 KV
0 VOLTS
0.002" STAINLESS STEEL WINDOW
ELECTRON LENS
TO COLD TRAP AND VACUUM PUMPS
RCA 7046
MU METAL SHIELD

scintillator optically coupled to an RCA 7046 photomultiplier. The fragment detectors were mounted on opposite sides of the lens with their axes coinciding with the vertical axis of the vacuum chamber. The distance from the center of the source to each fragment detector was 30 cm.

A pair of three-inch diameter, 0.002-inch thick stainless steel windows were provided to allow a horizontal neutron beam to enter one side of the chamber and exit on the other side. The horizontal axis, defined by these circular windows, intersected the vertical axis at the center of the source independent of the turntable position.

In addition to the source mounted on the central lens element, another source of fission fragments was included in this apparatus. This source consisted of a deposit of californium-252 on a 0.1 mg/cm^2 nickel foil. Californium-252 decays with a half-life for alpha-particle emission of 2.2 years and a spontaneous fission half-life of 60 years. This source, shown on the vertical axis directly below the turntable in Figs. 4 and 5, was mounted on a horizontal shaft. A rack and pinion, driven by a motor, allowed the source either to be positioned on the chamber axis or withdrawn, below the turntable, beyond the view of the top fragment detector. When the californium source was positioned on the axis, pulse-height distributions of electrons could be obtained for californium fragments entering the source mounted on the lens. Distributions obtained in this manner were useful not only for the measurements of the relative yield versus depth discussed in Chapter II, but also for periodic checks on the stability of the apparatus during extended periods of time.

The vacuum system consisted of a liquid-nitrogen cold trap, a water-cooled baffle, a diffusion pump, and a fore pump. With this system the pressure in the chamber under operating conditions was of the order

of 10^{-6} mm of Hg, which was sufficient to prevent high-voltage breakdown within the chamber.

Neutron Beam

A neutron beam from the Southwest Rotary Port of the Omega West Reactor was used in this experiment as shown in Fig. 6. This reactor is a light-water-moderated, heterogeneous reactor with a uranium-235 core. The SWR port views the core through a three inch thick beryllium moderator. The inner section of the port contained a six foot long graphite collimator with a two-inch diameter central hole. In the outer three feet, the beam was further restricted to one inch in diameter by a steel and Masonite collimator. This port was also provided with an eighteen-inch-long rotary shutter, which, when closed, was sufficient to reduce the radiation in the beam region at the reactor surface to a safe value.

The vacuum chamber was carefully positioned in front of the one-inch diameter hold in the face of the reactor with the horizontal axis of the chamber, defined above, coincident with the beam axis. The chamber and beam catcher, which consisted of alternate layers of steel and Masonite, were enclosed in a boron-loaded paraffin shield.

From subsequent measurements with sources of uranium-235 and uranium-238, estimates of the fluxes of both slow and fast neutrons emanating from this port were obtained. In the course of this determination, a knowledge of the shape of the neutron energy distribution was required. Since this distribution was not measured, the following assumptions were used: The slow neutron spectrum was Maxwellian, with a most probable velocity of 2200 m/sec. The energy distribution of the fast neutrons was

Fig. 6.--Horizontal cross section of the Omega West Reactor.

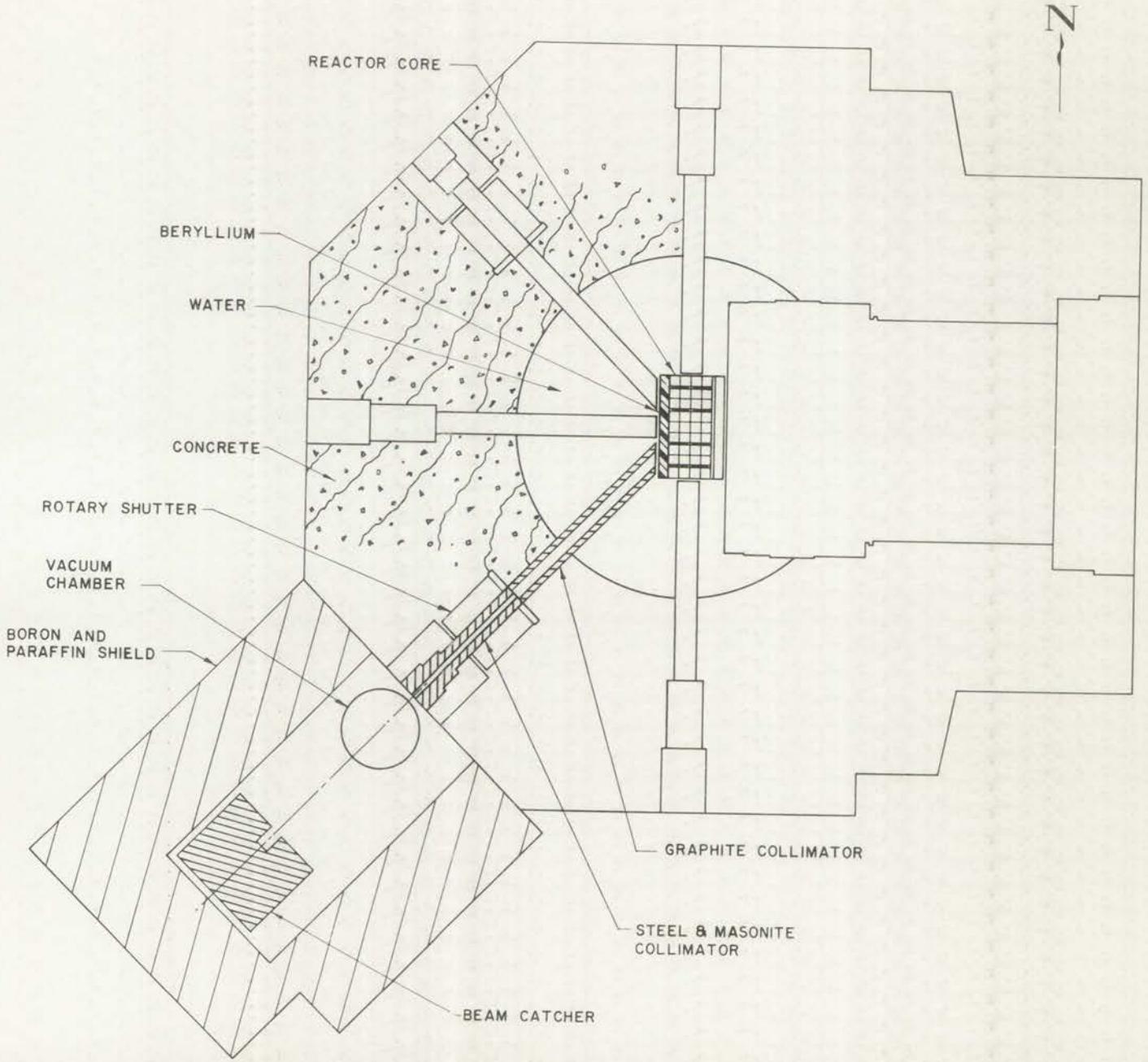
N
REACTOR CORE
BERYLLIUM
WATER
CONCRETE
ROTARY SHUTTER
VACUUM CHAMBER
BORON AND PARAFFIN SHIELD
GRAPHITE COLLIMATOR
STEEL & MASONITE COLLIMATOR
BEAM CATCHER

represented by a fission spectrum. The first assumption follows from the application of kinetic theory to the problem of neutrons in thermal equilibrium with atoms of the moderator and agrees with directly-measured velocity distributions.[17] The second assumption is considered reasonable in view of the results obtained by Evans[18] for the spectrum of fast neutrons from another water-moderated reactor. With these assumptions and the known fission cross sections, the fast and slow neutron fluxes were found to be comparable and approximately equal to 10^8 neutrons/cm^2-sec. In addition to neutrons, the beam contained a considerable flux of undesirable gamma rays which contributed to the background pulse rate of the scintillation detectors. To reduce this effect, a two-centimeter-thick lead absorber (not shown) was placed in the collimator, eighteen inches from the reactor face. This thickness was selected as a compromise between minimum background and maximum available fast neutron flux.

Operating Modes

With a source of fissile material mounted on the central lens element, two modes of operation of this apparatus were possible. First, with the neutron beam off and the californium source positioned on the vertical axis, hereafter referred to as the "in" position, it was possible to obtain the pulse-height distribution of electrons emitted by fragments entering the lens-mounted source. In the second mode of operation, the californium source was retracted to the "out" position and the port shutter rotated so that the neutron beam was incident on the fissile source. With this arrangement, it was possible to obtain the pulse-height distribution of electrons emitted by fragments emerging from the upper surface of this source. In the second mode of operation, two positions of the turntable

were of special interest. These two orientations are shown schematically in Fig. 7. In position 1, the neutrons were incident on the top surface of the source mounted on the lens, whereas in position 2, the neutrons were incident on the bottom surface.

Electronic Equipment

The following description of the electronic equipment is valid for either mode of operation. Pulses from each of the fragment detectors, within the proper time interval, established not only the occurrence of a fission event, but also whether the light or heavy fragment entered the top detector. A time-to-pulse-height converter was used for this purpose. Under normal operating conditions, a coincidence between the pulse from this converter and a pulse from the electron detector opened the gate on a three-channel pulse-height analyzer. This analyzer was capable of analyzing three pulses simultaneously and recording numerically the height of each pulse on a punched paper tape as well as a printed tape. While the three pulse heights were being recorded, the analyzer was disabled. Pulses from the electron detector and the time-to-pulse-height converter were fed into channels I and III of the analyzer, respectively. The overall amplification of the photomultiplier and amplifiers associated with the electron channel was stabilized by means of a gain stabilization circuit. Channel II of the analyzer was used periodically to monitor the operation of a part of this stabilization system.

Figure 8 shows a block diagram of the electronic equipment. Pulses from the top fragment detector were amplified by two Hewlett-Packard Model 460B distributed amplifiers. These pulses were used to start the

Fig. 7.--Schematic representation of the two turntable positions.

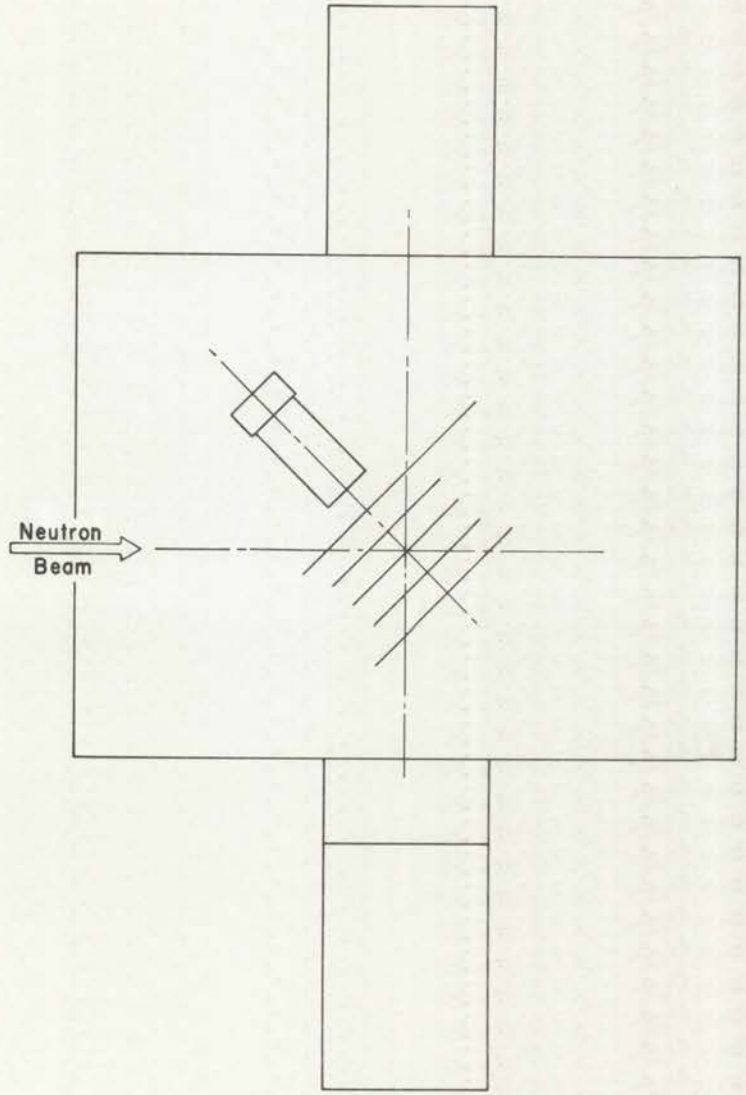

Position 1

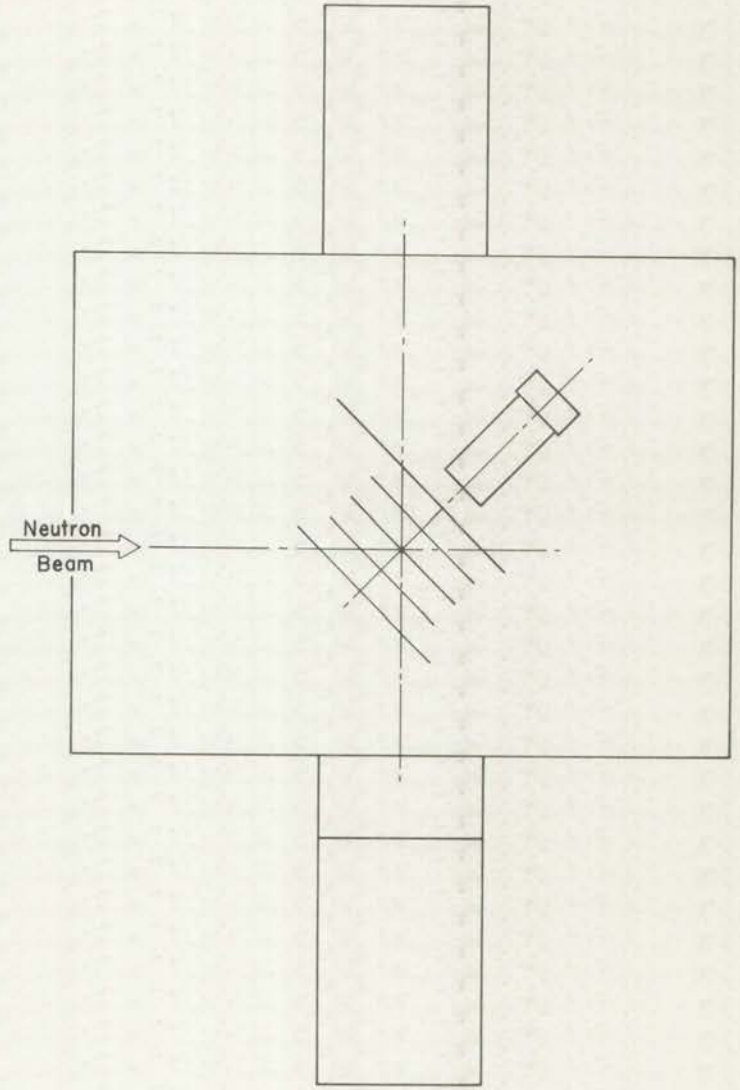

Position 2

Fig. 8.--Block diagram of the electronic apparatus.

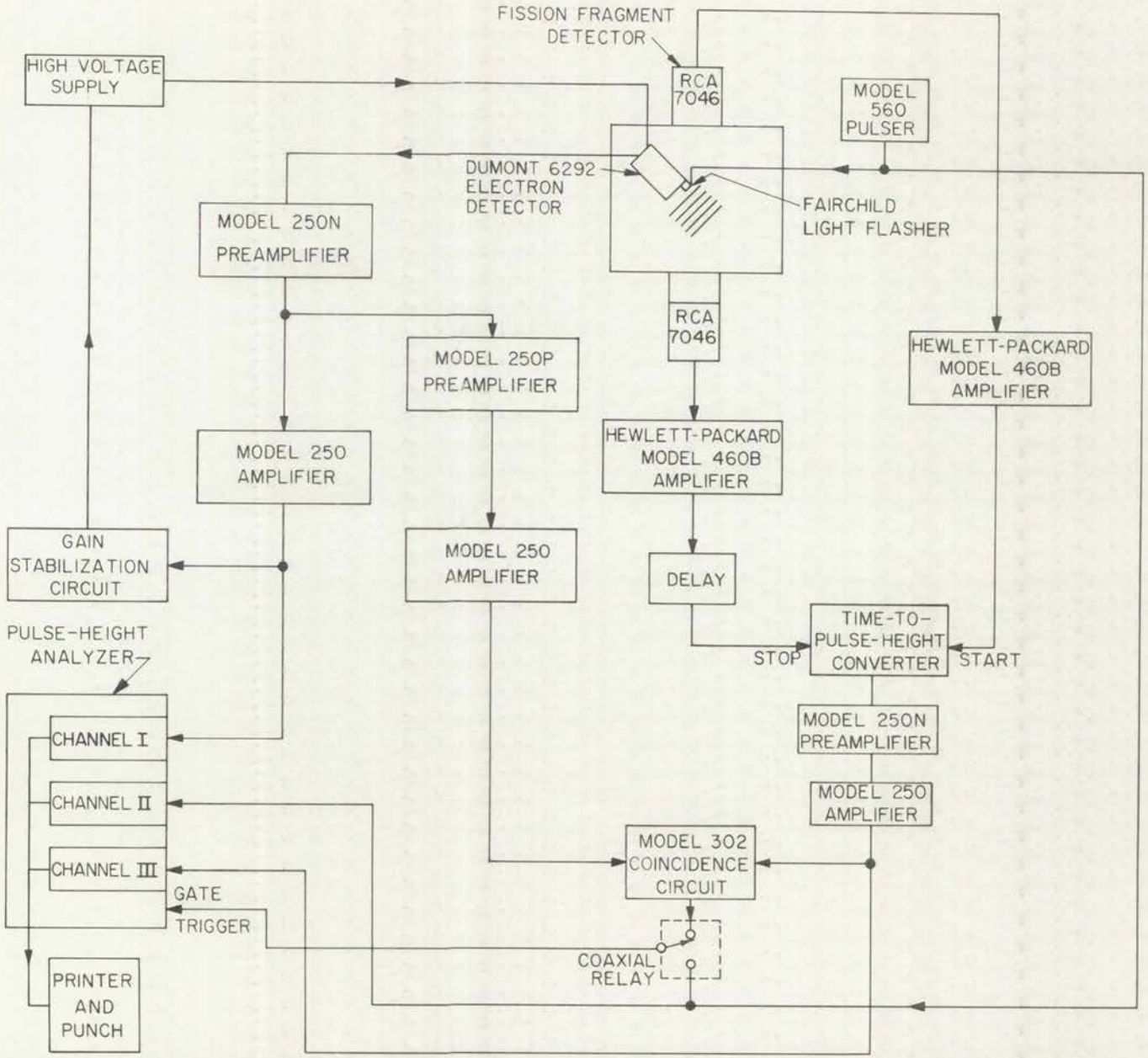
FISSION FRAGMENT DETECTOR
HIGH VOLTAGE SUPPLY
RCA 7046
MODEL 560 PULSER
DUMONT 6292 ELECTRON DETECTOR
FAIRCHILD LIGHT FLASHER
MODEL 250N PREAMPLIFIER
RCA 7046
MODEL 250P PREAMPLIFIER
HEWLETT-PACKARD MODEL 460B AMPLIFIER
MODEL 250 AMPLIFIER
HEWLETT-PACKARD MODEL 460B AMPLIFIER
GAIN STABILIZATION CIRCUIT
MODEL 250 AMPLIFIER
DELAY
PULSE-HEIGHT ANALYZER
TIME-TO-PULSE-HEIGHT CONVERTER
STOP
START
MODEL 250N PREAMPLIFIER
CHANNEL I
CHANNEL II
MODEL 250 AMPLIFIER
CHANNEL III
MODEL 302 COINCIDENCE CIRCUIT
GATE
TRIGGER
COAXIAL RELAY
PRINTER AND PUNCH

time-to-pulse-height converter. The pulses from the bottom fragment detector were similarly amplified and delayed by 0.1 μsec and were used to stop the converter. Los Alamos Model 250 amplifiers having a 0.25 μsec rise time and a delay-line shaped pulse width of 1.0 μsec were the type of amplifiers used in the remainder of the equipment. The Los Alamos Model 302 universal coincidence circuit contains two input channels, each having a pulse-height discriminator and a variable time-delay. The additional amplifiers in the electron detector channel were required to allow an independent amplitude adjustment of the pulse into the coincident circuit. Standard electronic high-voltage power supplies (some not shown) were used with the photomultipliers. The lens voltage was provided by a 2-20 kilovolt power supply. This supply contained a standard cell and a chopper amplifier for stabilization. Measurements showed that the output of this power supply was stable to 0.02% of the operating voltage. A negative lens voltage of 15 kilovolts was used for all measurements described in this work.

Gain Stabilization System

For proper operation, the gain stabilization circuit required a prominent peak in the pulse-height spectrum. Since a satisfactory peak was not available in the spectrum of pulses from the electron detector, an artificial peak had to be introduced. This was accomplished by means of solid-state light flashers mounted on the face of the electron detector, as shown in Fig. 4. Two Fairchild light flashers (FLP-1-F-6024) were connected in series and driven to breakdown by positive pulses. A schematic diagram of this arrangement is shown in Fig. 9b. Approximately 40-volt pulses with a repetition rate of 65 pulses/sec were obtained from a

Fig. 9.--Schematic diagram of the apparatus associated with the gain stabilization system.

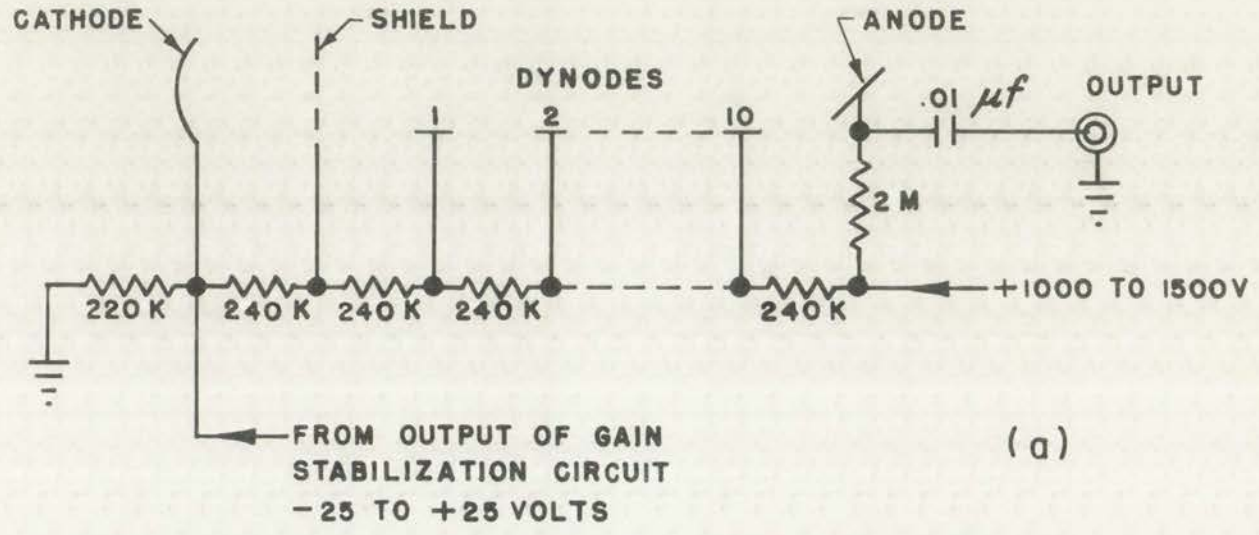
CATHODE
SHIELD
DYNODES
1
2
10
ANODE
.01 μf
OUTPUT
2 M
220 K
240 K
240 K
240 K
240 K
+1000 TO 1500V
FROM OUTPUT OF GAIN
STABILIZATION CIRCUIT
−25 TO +25 VOLTS

(a)

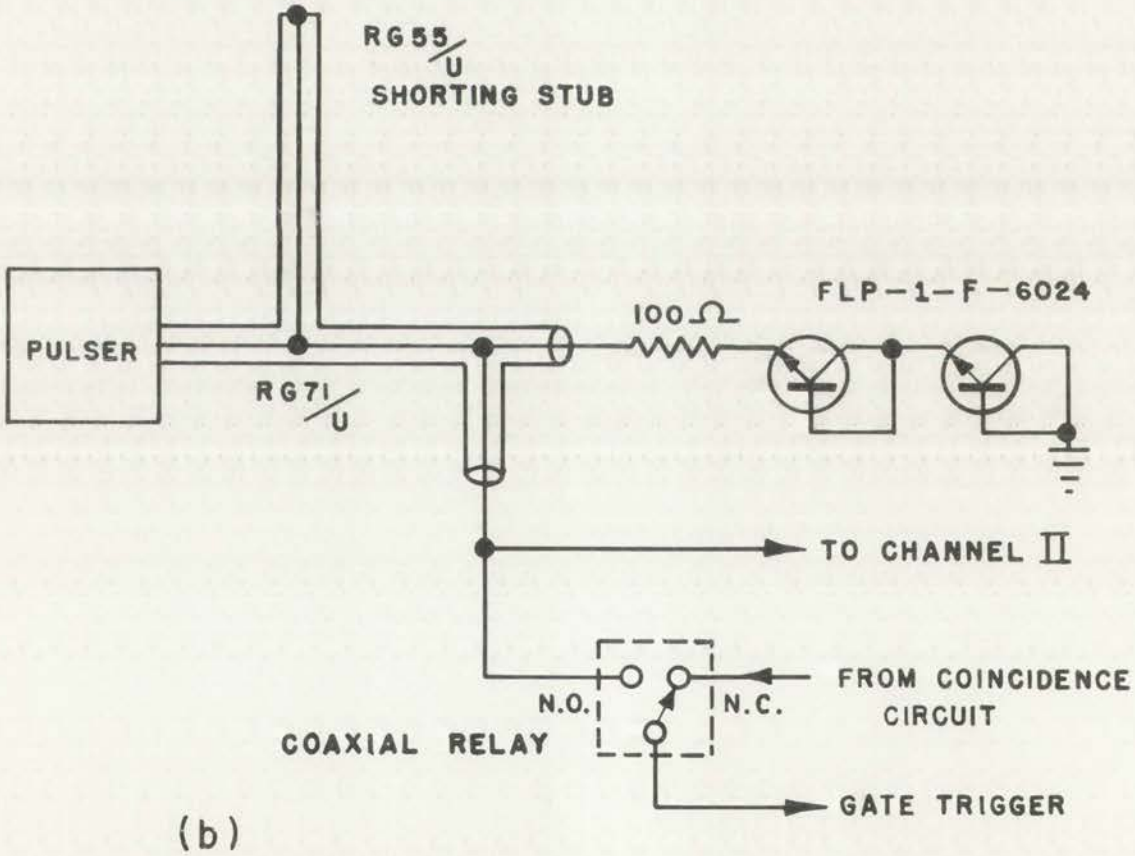
RG 55/U
SHORTING STUB
PULSER
RG 71/U
100 Ω
FLP−1−F−6024
TO CHANNEL II
FROM COINCIDENCE
CIRCUIT
N.O.
N.C.
COAXIAL RELAY
GATE TRIGGER

(b)

Los Alamos Model 560 pulser. These pulses were clipped to a width of 0.5 μsec by a shorting stub. A 100 ohm resistor was placed in series with the light flashers to limit their current.

The gain stabilization circuit used in this experiment was similar to the one described by H. de Waard.[19] This circuit consisted of a single channel analyzer followed by a counting-rate-difference circuit. Briefly, the operation was as follows: The single channel was positioned at the maximum of the peak on the pulse-height spectrum with a width comparable to the full-width at half-maximum of this peak. The threshold was modulated with a peak-to-peak voltage comparable in magnitude to the channel width. In this way, the single channel was swept back and forth across the peak with a repetition rate of 60 cycles per second. The counting-rate-difference circuit was gated by this same modulating signal. An output voltage was produced which was proportional to the difference between the counting rates which were present during the positive and negative half cycles of the modulating voltage. This output was added, with proper polarity, to the photomultiplier voltage in the manner shown in Fig. 9a. Thus, a change of the overall amplification of the electron detection system was counteracted by an almost equal, but opposite, change of the photomultiplier gain. Measurements showed that the gain stabilization of this system, which is defined as the ratio between the relative gain changes without and with stabilization, was approximately 30. The response time for an instantaneous gain change of one percent was found to be about 15 seconds.

This gain stabilization system was incomplete. In the first place, the feedback loop bypassed the scintillator and, therefore, did not include

the complete electron detector. If the characteristics of the scintillator changed, the pulse-height distribution would have shifted without a compensating change of the photomultiplier gain. In the second place, the system was dependent on the stability of the pulser and light flashers. Any instability in these components would have affected the stability of the entire electron detector channel. Fortunately, these effects were found to be small compared with the variation of the photomultiplier gain. This was determined from subsequent measurements of the average electron-pulse heights for californium fragments. Measurements were made at frequent intervals during a three-day period. These results indicated that the gain change of the electron-detector system was less than one tenth of one percent per hour under standard operating conditions.

Although the pulser contained a well-regulated power supply and was expected to be very stable, it was, nevertheless, monitored periodically. This was accomplished by means of the coaxial relay shown in Figs. 8 and 9b. With the relay arm connected to the normally open contact, a small fraction of the pulser signal was used as a gate trigger for the analyzer. In this condition, the pulses occurring in channels I and II were analyzed simultaneously. These data provided the pulse height not only of the pulse directly from the pulser, but also of the artificial peak produced by the light flasher.

Other circuits, not shown in the block diagram, were also used in this experiment. They consisted primarily of timers and relays to control the rotation of the turntable.

CHAPTER IV

MEASUREMENT OF THE AVERAGE PULSE HEIGHT VERSUS DEPTH

The variation of the electron yield with the depth of the origin of the fission event has been considered for fragment directions parallel to the surface normal in Chapter II. A qualitative theory was used to obtain an estimate of this function in terms of the characteristic lengths, L_δ', L_δ, and L_s. Unfortunately, the theory, in its present form, is incapable of predicting this function and the values of these lengths with sufficient accuracy to be of use in the present experiment. In addition, the nature of the present method requires that a measure of the yield be obtained for fragments whose directions are not parallel to the surface normal. The theory does not predict an angular dependence of the yield and, therefore, is not applicable to the conditions of this experiment. Here, the fragment direction is inclined at a 45 degree angle with respect to the foil normal. For these reasons, an independent measurement of the yield versus depth for conditions representative of those prevailing in the present experiment was required.

For this measurement, a set of calibration sources containing isotopes of uranium was used. These sources were constructed in the manner described in Appendix A and illustrated in Fig. 10. First, a layer ($\sim$1.4 $\mu g/cm^2$) of U-235 was deposited. Second, on all but one of

Fig. 10.--Construction of the calibration sources.

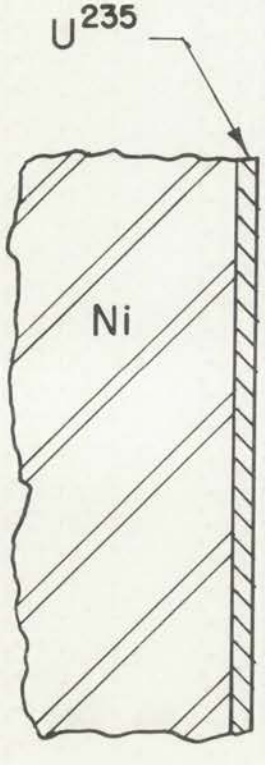

(a)

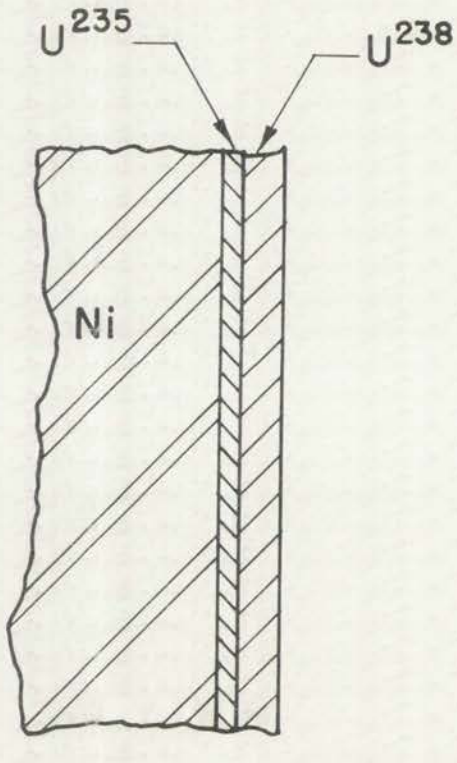

(b)

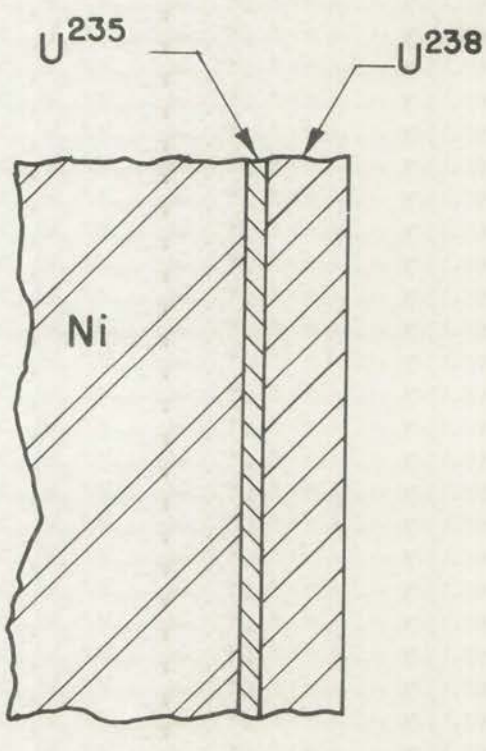

(c)

these foils, a layer of U-238 was deposited on top of the U-235 layer. The thicknesses of the U-238 layers were not constant and ranged from 1.4 $\mu g/cm^2$ for the thinnest to 10 $\mu g/cm^2$ for the thickest deposit. The uranium isotopes were in the form of uranium tetrafluoride and all depositions were made by vacuum evaporation. Immediately after the U-235 evaporation and before the U-238 was deposited, the emission rate of the natural alpha particles was measured for each foil. The U-235 thicknesses were then determined from the specific activity which had been measured previously for the same batch of material. A similar procedure was employed to determine the thickness of the U-238 deposit on each foil. However, in this case, the mask, which was placed over the foil to define the area of the deposit during the evaporation, was counted instead. A description of the foils used in this measurement is given in Table 1. Here the thicknesses of the layers are given in

TABLE 1

THICKNESSES OF THE URANIUM TETRAFLUORIDE LAYERS ON THE CALIBRATION SOURCES

Source Number	U^{235} Thickness		U^{238} Thickness		Total Thickness	
	$\mu g/cm^2$	q* (angstroms)	$\mu g/cm^2$	m* (angstroms)	$\mu g/cm^2$	ℓ* (angstroms)
4	1.4	30	0	0	1.4	30
13	1.4	30	1.4	30	2.8	60
14	1.5	32	2.4	51	3.9	83
10	1.0	21	2.8	59	3.8	80
9	1.4	30	4.4	93	5.8	123
16	1.7	36	6.4	135	8.1	171
18	1.1	23	10.0	211	11.1	234

*Slant thicknesses.

terms of the weight per unit area and also in angstroms. For this conversion, the value of the bulk density of UF_4, $\rho = 6.7\ g/cm^3$, given by Katz and Rabinowitch,[20] was adopted. In addition, the values given in angstroms are the thicknesses measured parallel to the foil normal times the square root of two, which correspond to the path lengths of the fission fragments within the uranium layers and are hereafter called "slant" thicknesses.

These foils were mounted on the central lens element in succession and measurements of the electron pulse-height distributions were obtained. Two such distributions were obtained for each source. First, with the neutron beam off and the californium source at the "in" position, an electron pulse height distribution was measured for californium fragments entering the source. Second, with the beam on and the californium source in the "out" position, a distribution was obtained for fission fragments emerging from the source. In this case, the fission of U-235 induced by the slow neutrons was the predominant source of fission fragments. Although either position of the turntable would have been acceptable, position 1 was used for these measurements. The electron pulse height distribution shown in Fig. 11a is representative of the data from channel I and the distribution shown in Fig. 11b is representative of the data from channel III. The two peaks in the latter curve are the consequence of the unequal mass split which is characteristic of fission processes encountered in this work. For equal distances, D, between the source and fragment detectors, the time between the occurrence of the start and stop pulses at the time-to-pulse-height converter is given by $t = T + D\,(1/V_b - 1/V_t)$, where V_t and V_b are the velocities of the

Fig. 11.--Typical pulse-height spectra.

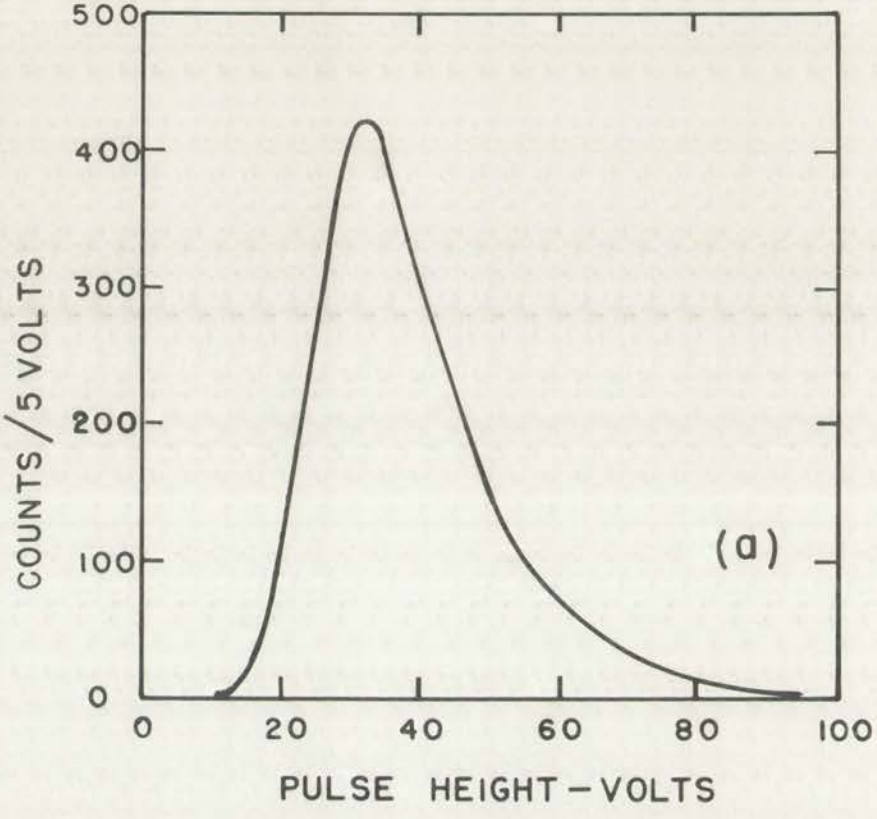
500
400
300
200
100
0
COUNTS/5 VOLTS
(a)
0
20
40
60
80
100
PULSE HEIGHT – VOLTS

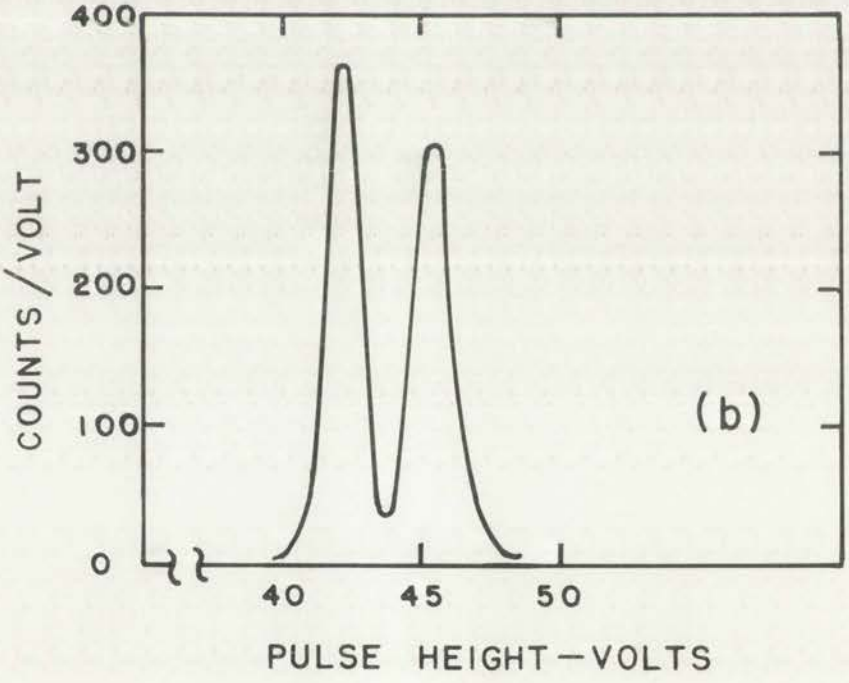
400
300
200
100
0
COUNTS / VOLT
(b)
40
45
50
PULSE HEIGHT – VOLTS

fragments detected by the top and bottom detectors, respectively. Also, T is given by $T = T_b - T_t$, where T_t and T_b are the time delays in the top and bottom circuits, respectively. If M_t and M_b represent the corresponding fragment masses, the momentum principle gives $M_t V_t = M_b V_b$. Since the probability of fission for the symmetric mode is negligible, the number of events recorded when $M_t = M_b$ or when $V_t = V_b$ is a minimum. In this case $t = T$. For asymmetric modes, the yield reaches a maximum for mass ratios and, therefore, velocity ratios in the region of 1.4 . For these modes, the most probable velocities of the light and heavy fragments are $V_L = 1.4 \times 10^9$ cm/sec and $V_H = 0.96 \times 10^9$ cm/sec. If the light fragment is incident on the top detector, V_t is equal to V_L and $t = T + 0.4\ D/V_L$. If, however, $V_b = V_L$, then $t = T - 0.4\ D/V_L$. Thus, the separation of these peaks is given by $\Delta t = 0.8\ D/V_L$ which, for the conditions encountered in this experiment, has the value $\Delta t \approx 17$ μsec. The decrease of the fission yield for mass ratios larger than about 1.4 is reflected in the decrease of the time spectrum for larger and smaller values of t. Since the output pulse height of the converter is related linearly to the time between the arrival of the start and stop pulses, the pulse-height spectrum is similar to the time spectrum. In this experiment, the fission events are grouped into two categories which correspond to the two peaks of the channel III distribution. Those events which correspond to the higher peak are associated with fissions in which the light fragment is emitted in the upward direction. Those events corresponding to the lower peak are associated with fissions in which the light fragment is emitted in the downward direction.

A nine digit number is punched on the paper tape by the analyzer for each recorded fission event. The first three digits (0-199) give the height of the pulse in channel I and the last three digits represent the height of the pulse in channel III. These data are transferred to magnetic tape which serves as a data-input tape for the IBM 704 Electronic Computer. The computer determines the average and the width of the electron-pulse-height distribution for the light and heavy fragments separately.

For the first series of measurements, all of the sources listed in Table 1 with the exception of source #10 were used. In addition, source #29, which was a blank nickel foil, was included in this set. The uranium sources were selected in the order of increasing total uranium thickness and were mounted in succession on the central lens element. Source #29 was taken last. Data were obtained separately for californium and uranium fission fragments for all sources except #29. In the case of the blank nickel, data were taken for californium fragments with the neutron beam off and also with the beam on. Including the time necessary to evacuate the chamber and to allow the electronics to stabilize after each foil change, the total time required for the measurements on each source was approximately one day. A total of ten days was required to complete these measurements.

Results for the californium fragments are given in Table 2 and Fig. 12. Here, the average-electron-pulse heights for heavy and light californium fragments entering the sources are represented by C_H and C_L, respectively, and the average of C_H and C_L with equal weighting is represented by C. The uncertainties are the standard statistical error of the mean. The results for source #29 showed that the gain of the electron

Fig. 12.--Average electron-pulse height as a function of the total slant thickness.

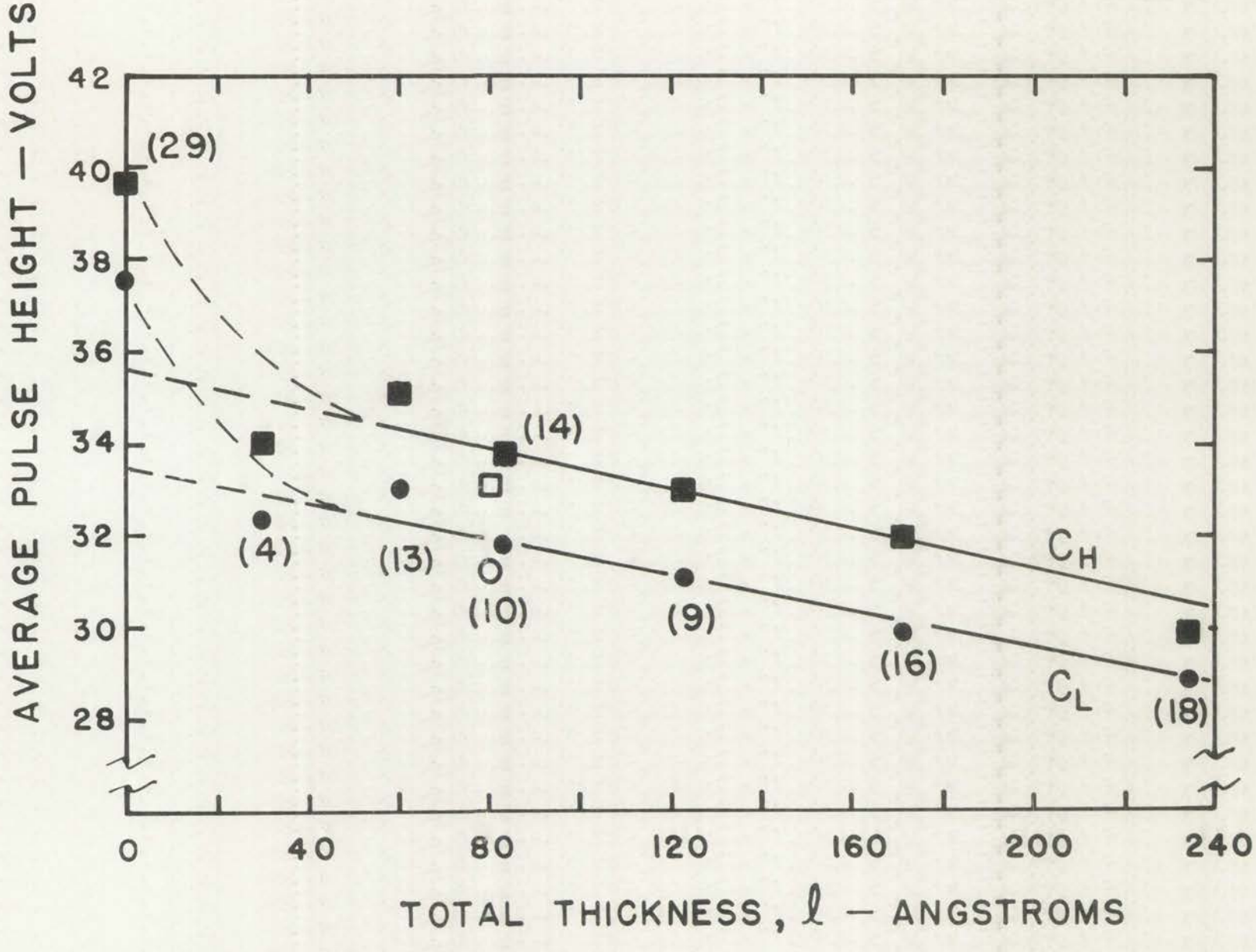
AVERAGE PULSE HEIGHT — VOLTS
42
40
38
36
34
32
30
28
(29)
(14)
(4)
(13)
(10)
(9)
(16)
(18)
C_H
C_L
0
40
80
120
160
200
240
TOTAL THICKNESS, ℓ — ANGSTROMS

TABLE 2

AVERAGE ELECTRON-PULSE HEIGHTS FOR CALIFORNIUM FRAGMENTS ENTERING THE CALIBRATION SOURCES

Source Number	Pulse Height in Volts		
	C_H	C_L	C
4	34.0 ± 0.2	32.2 ± 0.2	33.2 ± 0.2
13	35.1 ± 0.2	33.0 ± 0.2	34.0 ± 0.2
14	33.7 ± 0.2	31.8 ± 0.2	32.7 ± 0.2
9	33.0 ± 0.2	31.1 ± 0.2	32.1 ± 0.2
16	32.0 ± 0.2	29.9 ± 0.2	31.0 ± 0.2
18	29.9 ± 0.2	28.9 ± 0.2	29.4 ± 0.2
29[a]	39.7 ± 0.3	37.5 ± 0.2	38.6 ± 0.2
29[b]	38.8 ± 0.2	36.9 ± 0.2	37.9 ± 0.2

[a]Neutron beam off.

[b]Neutron beam on.

detector channel was 1.9 percent higher with the beam off than it was with the beam on. Subsequent measurements revealed that the difficulty was in the pulse-height analyzer. The output of this analyzer was found to be slightly dependent on the total counting rate which was many orders of magnitude larger with the beam on than it was with the beam off. All data obtained with uranium fragments were increased by 1.9 percent to correct for this gain change. The uranium fragment data are presented in Table 3, where u and U indicate observed and corrected average pulse heights. The subscripts H and L refer to heavy and light fragments emerging from the surface of the source.

A second series of measurements was made at a later time.

TABLE 3

AVERAGE ELECTRON-PULSE HEIGHTS FOR URANIUM FRAGMENTS EMERGING FROM THE CALIBRATION SOURCES

Source Number	Pulse Height in Volts					
	u_H Observed	U_H Corrected	u_L Observed	U_L Corrected	u Observed	U Corrected
4	44.4 ± 0.3	45.3 ± 0.39	36.5 ± 0.24	37.2 ± 0.3	40.5 ± 0.2	41.2 ± 0.3
13	47.7 ± 0.2	48.6 ± 0.39	38.5 ± 0.23	39.3 ± 0.3	43.1 ± 0.2	43.9 ± 0.2
14	49.7 ± 0.3	50.6 ± 0.43	39.3 ± 0.25	40.0 ± 0.4	44.5 ± 0.2	45.3 ± 0.4
9	48.2 ± 0.2	49.1 ± 0.40	38.1 ± 0.22	38.8 ± 0.3	43.2 ± 0.2	44.9 ± 0.3
16	49.9 ± 0.2	49.9 ± 0.40	38.7 ± 0.22	39.4 ± 0.3	43.8 ± 0.2	44.7 ± 0.3
18	44.7 ± 0.2	45.6 ± 0.38	37.4 ± 0.22	38.2 ± 0.3	41.1 ± 0.2	41.9 ± 0.3

Sources numbered 10, 18, 14, 29 and 8 were measured in the order given. Source #8 was another blank nickel foil. The purpose of this series of measurements was as follows: (1) to include data from source #10, (2) to obtain data from sources numbered 18 and 14 in an order reversed from the first series to check for a possible gain change during the previous measurements, and (3) to compare the results from two blank foils which, as far as this experiment is concerned, are considered to be identical. The results of these measurements are given in Table 4.

From a comparison of the values given in Tables 2 and 4 for sources #14 and #18, it is evident that the gain was about 3 percent lower for the second series of measurements. Therefore, the californium results for source #10 were increased by 3 percent before they were included in Fig. 12. The above comparison also showed that the gain drift during the first series of measurements was insignificant and, therefore, no correction was required. The results for the two blank nickel sources, likewise, agreed to within 2 or 3 percent.

Figure 12 contains the average pulse heights for californium fragments plotted against the total slant thickness, ℓ. The numbers in parentheses identify the source from which the pulse-height data were obtained. The pulse heights decreased rapidly from the values for blank nickel to the values for the thinnest UF_4 layers. This is considered to be an indication that the uranium tetrafluoride was deposited more or less uniformly and did not consist of large well-separated agglomerates. A slower decrease of the average pulse heights with an increase in thickness of the deposit is also apparent. A possible explanation for this effect is as follows: Electron micrographs of uranium surfaces

TABLE 4

RESULTS OF THE SECOND SERIES OF MEASUREMENTS

Source Number	Pulse Height in Volts					
	C_H	C_L	C	u_H	u_L	u
10	32.1 ± 0.2	30.2 ± 0.2	31.1 ± 0.2	45.9 ± 0.3	35.9 ± 0.2	40.9 ± 0.2
18	28.7 ± 0.2	27.5 ± 0.2	28.1 ± 0.1	43.2 ± 0.2	36.0 ± 0.2	39.6 ± 0.2
14	33.0 ± 0.2	31.3 ± 0.2	32.2 ± 0.2	48.1 ± 0.3	38.3 ± 0.2	43.2 ± 0.2
29	37.3 ± 0.2	35.4 ± 0.2	36.3 ± 0.2			
8	36.4 ± 0.2	34.4 ± 0.2	35.4 ± 0.2			

prepared by vacuum evaporation show that the surface roughness increases for thicker deposits.[21] The influence of the surface structure on the yield, in the case of secondary electron emission, has been discussed by Bruining.[22] In this case, the yield was observed to decrease with increasing roughness of the surface. In view of the similarity of the two processes, it is expected that the electron yield for fission fragments would follow the same pattern.

Another feature of these data, which is apparent not only for the californium results but also for the uranium data, is that the pulse heights observed for the heavy fragments are consistently larger than those obtained for the light fragments. This is undoubtedly a reflection of the greater rate of energy loss of the heavy fragments in the initial part of their range.[23]

Of particular interest, for the present experiment, are the relative average pulse heights which were obtained by dividing the values of U_H, U_L and U by the average pulse height for all californium fragments, C. These relative pulse heights are given in Table 5, where the uncertainties are the statistical standard deviations obtained by propagation of the errors. These data are also shown in Fig. 13, where the abscissa is the slant thickness of the U-238 layer, m. The errors shown are two standard deviations. These uncertainties were obtained from a comparison of the results from sources #10 and #14 and appear to be a more reasonable estimate of the actual errors involved in these measurements.

The shape of the curve for U/C versus m suggests that the relative pulse height for fragments originating at slant depth x, H(x), can be represented by the empirical function,

$$H(x) = A' - B' \exp(-x/g) \qquad (29)$$

Fig. 13.--Relative average-pulse height as a function of the uranium-238 slant thickness.

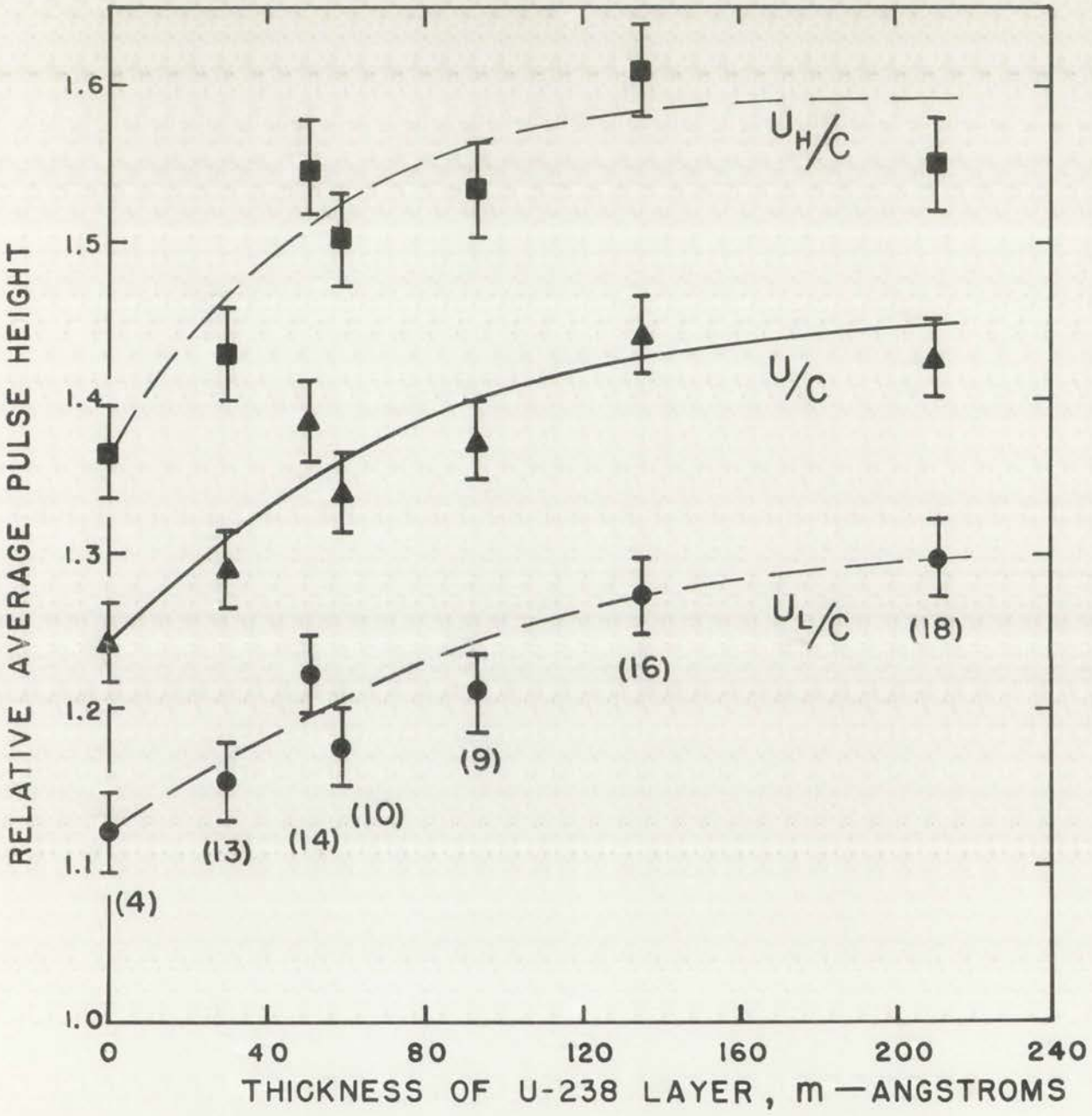
RELATIVE AVERAGE PULSE HEIGHT
1.6
1.5
1.4
1.3
1.2
1.1
1.0
U_H/C
U/C
U_L/C
(4)
(13)
(14)
(10)
(9)
(16)
(18)
0
40
80
120
160
200
240
THICKNESS OF U-238 LAYER, m — ANGSTROMS

TABLE 5

RATIOS OF THE AVERAGE PULSE HEIGHTS OBTAINED FROM THE CALIBRATION SOURCES WITH URANIUM AND CALIFORNIUM FISSION FRAGMENTS

Source Number	Relative-Average-Pulse Height		
	U_H/C	U_L/C	U/C
4	1.36 ± 0.01	1.12 ± 0.01	1.24 ± 0.01
13	1.43 ± 0.01	1.15 ± 0.01	1.29 ± 0.01
14	1.55 ± 0.02	1.22 ± 0.01	1.38 ± 0.01
10	1.50 ± 0.02	1.18 ± 0.01	1.34 ± 0.01
9	1.53 ± 0.02	1.21 ± 0.01	1.37 ± 0.01
16	1.61 ± 0.02	1.27 ± 0.01	1.44 ± 0.01
18	1.55 ± 0.02	1.30 ± 0.01	1.42 ± 0.01

where A', B' and g are constants. With this representation,

$$U/C = \int_m^{m+q} H(x)\, dx \Big/ \int_m^{m+q} dx \ , \tag{30}$$

which gives

$$U/C = A' - B'(g/q)[1 - \exp(-q/g)] \exp(-m/g) \tag{31}$$

or

$$U/C = A'' - B'' \exp(-m/g) \ ,$$

where $A'' = A'$ and $B'' = B'(g/q)[1 - \exp(-q/g)]$.

An adequate fit to the experimental data was found for A" = 1.47, B" = 0.23, and g = 80 angstroms. The solid curve in Fig. 13 was obtained by a substitution of these values into Eq. (31). With q equal to 30 angstroms, the values of A' and B' were readily found to be A' = 1.47 and B' = 0.27. These expressions give the average electron pulse height for uranium fragments relative to the pulse height for californium fragments.

To obtain the pulse height relative to uranium fragments, it is necessary merely to divide by the value of $H(x)$ evaluated at $x = 0$. Thus the relative-average-pulse height for uranium fragments as a function of the depth is

$$H(x)/H(0) = A - B \exp(-x/g) , \qquad (32)$$

where

$$A = A'/(A' - B') = 1.23 \text{ and } B = B'/(A' - B') = 0.23 .$$

A plot of $H(x)/H(0)$ with these values of the constants A and B is shown in Fig. 14.

With the assumption that the electron pulse height is proportional to the number of electrons,

$N(x)/N(0) = A - B \exp(-x/g)$. This is the empirical analogue of the function discussed in Chapter II.

Fig. 14.--Relative pulse height as a function of slant depth.

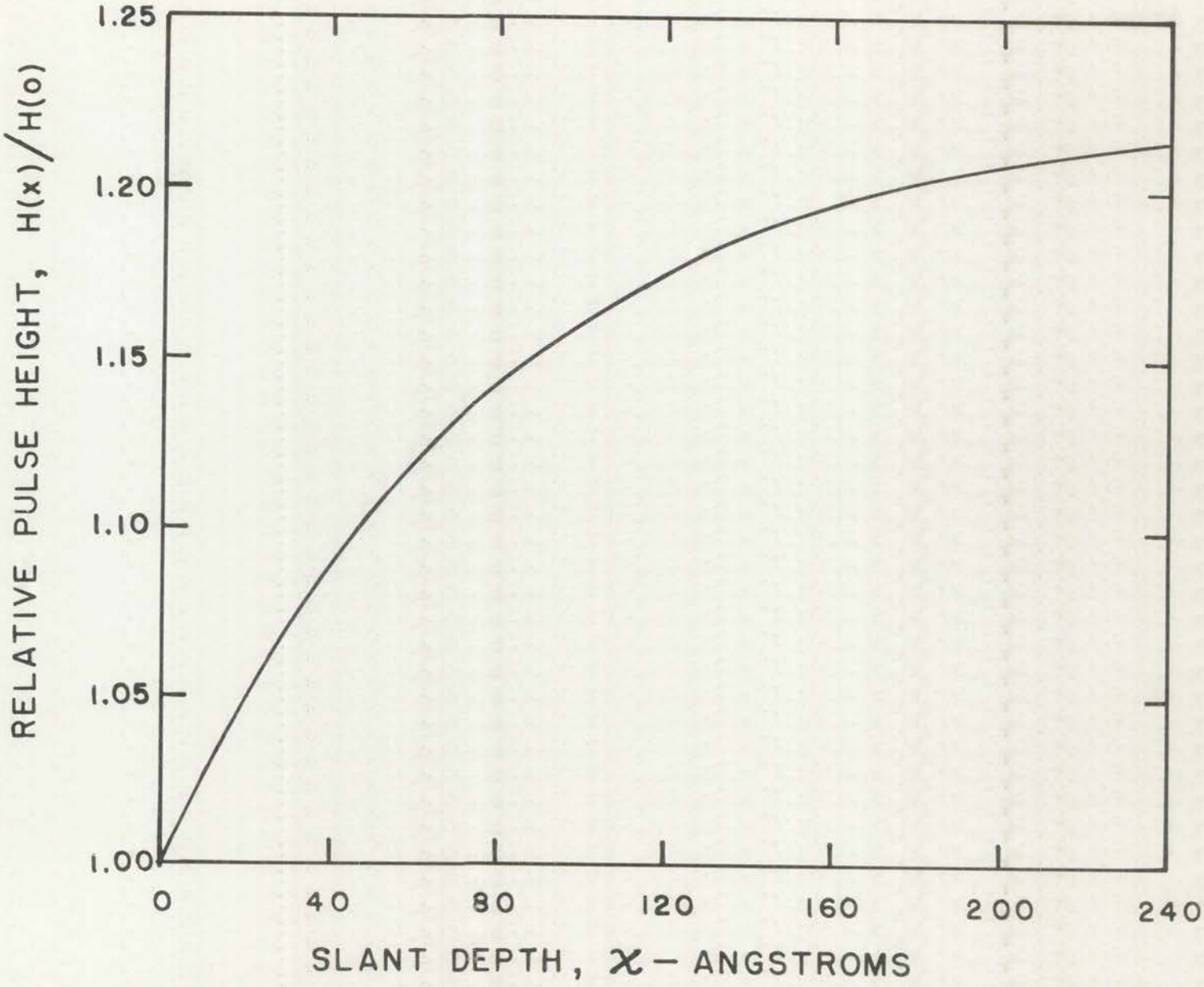
1.25
1.20
1.15
1.10
1.05
1.00
RELATIVE PULSE HEIGHT, H(x)/H(0)
0
40
80
120
160
200
240
SLANT DEPTH, x — ANGSTROMS

CHAPTER V

MEASUREMENT OF THE MEAN LIFETIME

This chapter contains a detailed description of the present method. In this description, the empirical expression for the relative-pulse height versus depth is used to obtain the relationship between the mean lifetime of a compound nucleus and average-pulse heights observed in this experiment. The necessary corrections which must be applied to the observed data are discussed. A description of the procedures that were followed to obtain the corrected-relative-pulse heights and their uncertainties is given, and the results obtained with sources of U-238 and Np-237 are presented. The possibility of a change in the source characteristics, which might have occurred during the extended irradiations, is considered, and the results of an auxiliary measurement designed to test this possibility are presented. Finally, the present method is evaluated and the results are discussed.

Detailed Description of the Method

Consider a fissile source mounted on the central lens element. This source consists of a layer of fissile material of thickness L deposited on a nickel foil and supported in the manner described in Appendix A. The orientation of this foil with respect to the direction of the neutron beam is shown for the two turntable positions, in Fig. 15. Although this discussion applies specifically to a neutron beam from a reactor, it is applicable to other sources of fast neutrons with sufficient

Fig. 15.--Enlarged view of the fissile layer.

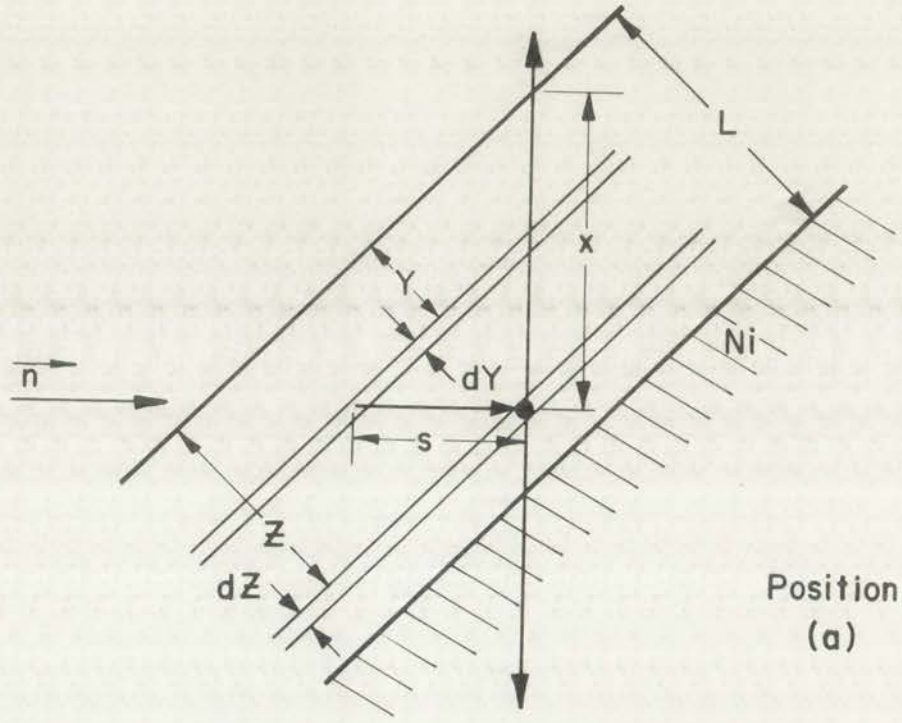

Position 1
(a)

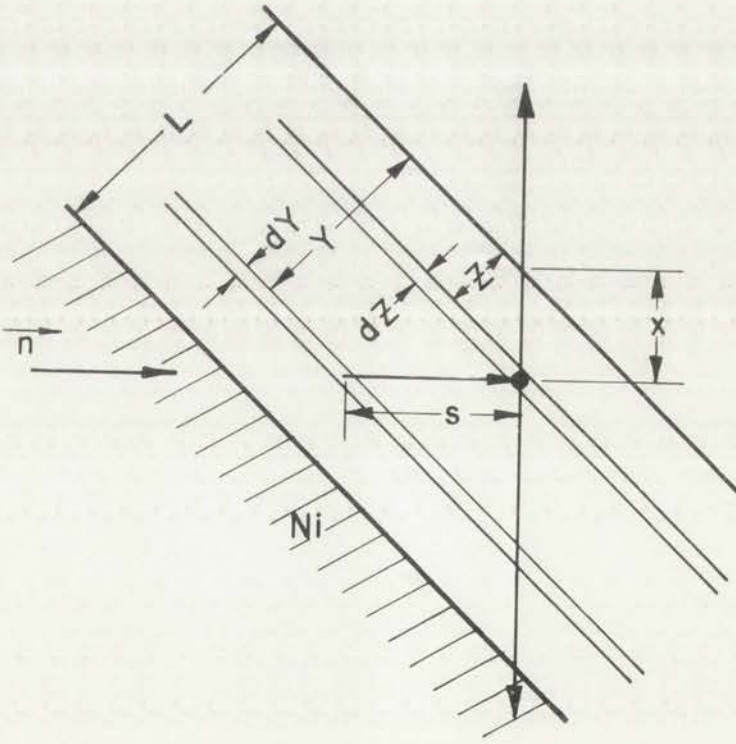

Position 2
(b)

intensity as well. In fact, some of the difficulties encountered in this experiment could have been circumvented if a sufficiently intense source of monoenergetic neutrons had been available.

Compound nuclei formed by fast neutron capture have an initial recoil velocity given by $v_c = \mu v_n/(M + \mu)$, where μ and M are the mass of the neutron and target nucleus, respectively, and v_n is the neutron velocity. These particles, in traversing the material in which they are formed, begin to lose kinetic energy immediately; hence, if fission occurs before they are brought to rest, the average recoil velocity is dependent upon the nuclear lifetime. If, however, the fission occurs in the initial part of the range, the average velocity is essentially equal to the initial velocity. In the case of a 12-kev uranium nucleus, the range is expected to be about 40A according to the (γ,n) recoil measurements reported by Schmitt et al.[24] Since this distance is about four times the mean recoil distance before fission expected in this measurement, the initial recoil velocity will be used in the following work.

Figure 15a shows the neutron beam, with direction $\vec{n}$, incident on the fissile surface of the source. The compound nuclei which are formed are driven away from the foil surface as shown by the vector with length s. The terminus of this vector is the origin of the fission event which is indicated by the solid circle. The two vectors originating from this point represent the directions of the detected fission fragments. Here, the fragments are considered to be colinear. The effect of a nonzero momentum of the center of mass, which actually causes the fragments to be non-colinear, will be considered later.

Let the neutron flux and the fission cross section be represented,

respectively, by $\Phi(E)$ and $\sigma_f(E)$, where each is a function of the neutron energy E. The energy spectrum of neutrons which are effective in this experiment, S(E), is proportional to $\Phi(E)\sigma_f(E)$. In the present discussion, S(E) is assumed to be normalized so that $\int_0^\infty S(E)dE = 1$.

Average Electron-Pulse Height for Position 1

Consider a neutron with energy E which is captured within the fissile layer with thickness L. Let the probability of capture per unit distance at depth Y be represented by K(Y). If the attenuation of the neutron beam is neglected, K is independent of the depth, Y, and is given by

$$\int_0^L K\,dY = 1 \text{ and } K = 1/L. \tag{33}$$

The normalized probability for fission at time t per unit time interval is the usual exponential decay given by

$$J(E,t) = \exp(-t/\tau)/\tau\ , \tag{34}$$

where τ is the mean lifetime of the compound nucleus which is expected to be a function of the excitation energy and, therefore, a function of the neutron energy, E. The corresponding probability for a recoil distance s per unit distance is given by

$$G(E,s) = \exp(-s/k)/k\ , \tag{35}$$

where k is the distance traversed by a compound nucleus with velocity v_c in time t and is given by $k = v_c t$. The relationship between the velocity of the nucleus and the neutron energy is given by $v_c = (2\mu E)^{\frac{1}{2}}/(M+\mu)$, so that k has the form $k(E) = (2\mu E)^{\frac{1}{2}}\,\tau(E)/(M+\mu)$. The probability of capture at

depth Y and fission in unit distance at depth Z is, therefore,

$$F(E,Z - Y) = K\,G(E,Z - Y) = (2^{\frac{1}{2}}/Lk)\exp[-2^{\frac{1}{2}}(Z - Y)/k]. \quad (36)$$

The probability of a fission event a depth Z per unit distance is

$$U_1(E,Z) = \int_0^Z F(E,Z - Y)dY;\ 0 \leq Z \leq L \quad (37a)$$

and

$$U_2(E,Z) = \int_0^L F(E,Z - Y)dY;\ Z \geq L. \quad (37b)$$

The results of these integrations are

$$U_1(E,Z) = (1/L)[1 - \exp(-2^{\frac{1}{2}}Z/k)];\ 0 \leq Z \leq L \quad (38a)$$

and

$$U_2(E,Z) = (1/L)[\exp(2^{\frac{1}{2}}L/k) - 1]\exp(-2^{\frac{1}{2}}Z/k);\ Z \geq L\ . \quad (38b)$$

From Fig. 15, the slant depth $x = 2^{\frac{1}{2}}Z$ and the slant thickness of the fissile layer, $\ell = 2^{\frac{1}{2}}L$. Therefore, Eqs. (38a) and (38b) become

$$U_1(E,x) = (1/\ell)[1 - \exp(-x/k)];\ 0 \leq x \leq L \quad (39a)$$

$$U_2(E,x) = (1/\ell)[\exp(\ell/k) - 1]\exp(-x/k);\ x \geq \ell\ , \quad (39b)$$

where, now, $U_1(E,x)$ and $U_2(E,x)$ are the probabilities of fission at depth x per unit slant distance. Let $Q(x,\xi)$ represent the normalized electron pulse-height distribution for fission events originating at slant depth x. Therefore, the probability that the fission event occurs at x and gives a pulse height ξ per unit distance and pulse-height interval is

$$W(E,x,\xi) = \begin{cases} U_1(E,x)\ Q(x,\xi);\ 0 \leq x \leq \ell \\ \\ U_2(E,x)\ Q(x,\xi);\ x \geq \ell\ . \end{cases} \quad (40)$$

The probability $P(E,\xi)$ that a neutron with energy E captured within the fissile layer ultimately leads to a pulse height ξ per unit pulse-height interval is obtained by an integration over x and a summation of the contributions. This gives

$$P(E,\xi) = \int_0^{\ell} U_1 Q dx + \int_{\ell}^{\infty} U_2 Q dx \ . \tag{41}$$

The average pulse height is

$$\bar{\xi}(E) = \int_0^{\infty} \xi \ P(E,\xi) \ d\xi$$

$$\bar{\xi}(E) = \int_0^{\ell} U_1 \left[\int_0^{\infty} \xi \ Q \ d\xi\right] d \ x + \int_{\ell}^{\infty} U_2 \left[\int_0^{\infty} \xi \ Q \ d\xi\right] dx \ . \tag{42}$$

The integral within the brackets is merely the average pulse height for fission events which originate at depth x. In terms of the previous notation,

$$\int_0^{\infty} \xi \ Q \ d\xi = H(x) \ .$$

Although it is not strictly applicable,[25] the result of the previous chapter will be used here not only in the region $0 \leq x \leq \ell$ but also for $x > \ell$. Therefore, from Eq. (32)

$$\int_0^{\infty} \xi \ Q \ d\xi = H(0) \ [A - B \exp(- x/g)] \ .$$

After this substitution the integrations give

$$\bar{\xi}(E) = H(0) \left\{ A - [Bg^2/\ell \ (k + g)] \ [1 - \exp(-\ell/g)] \right\} \ . \tag{43}$$

The pulse height, for the turntable in position 1, averaged over all effective neutron energies is

$$\langle \bar{\xi}(E) \rangle_1 = \int_0^\infty \bar{\xi}(E) S(E) dE \ . \qquad (45)$$

In order to evaluate this integral exactly, a knowledge of the dependence of k and therefore of τ on E is required. In the absence of this information, the value of this integral can be found only approximately. This was done in the following manner:

First, expand $\bar{\xi}(E)$ in a Taylor's series which gives

$$\bar{\xi}(E) = \bar{\xi}(\bar{E}) + (E - \bar{E})\bar{\xi}'(\bar{E}) + (E - \bar{E})^2 \bar{\xi}''(\bar{E})/2 + \ldots ,$$

where $\bar{E}$ is the average neutron energy. Second, calculate the average of each term of the series which gives

$$\langle \bar{\xi}(E) \rangle = \bar{\xi}(\bar{E}) + \langle (E - \bar{E})^2 \rangle \bar{\xi}''(\bar{E})/2 + \ldots .$$

As a first approximation, it will be assumed that the first term is dominant and that $\langle \bar{\xi}(E) \rangle = \bar{\xi}(\bar{E})$. With this assumption, which is justified in Appendix B, the average pulse height is given by

$$\langle \bar{\xi}(E) \rangle_1 = H(O) \left\{ A - [B\, g^2/\ell(\bar{k} + g)] \, [1 - \exp(-\ell/g)] \right\} , \qquad (46)$$

where $\bar{k} = \hat{v}_c \tau(\bar{E})$. Here, $\hat{v}_c$ is the recoil velocity of the compound nucleus formed by the capture of a neutron with energy $\bar{E}$ and is given by $\hat{v}_c = (2\mu\bar{E})^{\frac{1}{2}}/(M + \mu)$.

Average Electron-Pulse Height for Position 2

Figure 15b shows the source in position 2 where the neutrons are incident on the bottom side of the fissile layer. With the source in this position, the compound nuclei are driven towards the surface.

A fraction, f, of the nuclei are expected to escape from the fissile layer and subsequently fission in the region above the surface. For these events, the electrons are emitted by the downward directed fragments which enter the surface of the source. The contribution made by these fragments to the average electron pulse height is given by fH(0). Otherwise, this calculation of the average pulse height for the turntable in position 2 is similar to the previous one and gives

$$\langle \xi(E) \rangle_2 = H(0) \left\{ A + [B\bar{k}^2/\ell(g - \bar{k})][1 - \exp(-\ell/\bar{k})] \right.$$
$$\left. -[B\, g^2/\ell(g - \bar{k})][1 - \exp(-\ell/g)] \right\} \qquad (47)$$

Ratio of the Average Electron-Pulse Heights

The ratio of these pulse heights which is defined by

$$R = \langle \bar{\xi}(E) \rangle_1 / \langle \bar{\xi}(E) \rangle_2 \qquad (48)$$

is of particular importance in the present work. Besides the known parameters A, B, ℓ, and g, the ratio, R, is a function of $\bar{k}$. For $\bar{k}$ very much smaller than both g and ℓ, which is valid for the present experiment,

$$R(\bar{k}) \approx 1 + 2\, B_1 \bar{k}/\ell \ , \qquad (49)$$

where the constant $B_1 = B/\left\{ A - (Bg/\ell)[1 - \exp(-\ell/g)] \right\}$. Thus, R is expected to be a linear function of $\bar{k}$ in the region of present interest.

The measured quantity, in this experiment, is the ratio, R, from which the value of τ is found from Eq. (48). All the parameters

in this equation have been determined except for the thickness of the fissile layer, ℓ. It is easily seen that there is an optimum thickness for which the sensitivity of this experiment is a maximum. Equation (49) can be written in the form

$$\bar{k} \approx \alpha(R - 1) , \tag{50}$$

where $\alpha = \ell/2B_1$. The error associated with the ratio measurement, ΔR, is proportional to the error of the pulse height measurements, $\Delta\xi$, which, in turn, is given by $\Delta\xi \sim \sigma/\nu^{\frac{1}{2}}$, where σ is the standard deviation of the electron pulse height distribution and ν is the number of events contained in this distribution. For a given flux of neutrons, the number of events is proportional to the thickness of the fissile layer. Therefore, $\Delta R \sim 1/\ell^{\frac{1}{2}}$. The error of $\bar{k}$ is represented by $\Delta\bar{k}$ and is given by $\Delta\bar{k} = \alpha\Delta R$. For the greatest sensitivity, it is desired to have $\bar{k}/\Delta\bar{k} \sim (R - 1)\ell^{\frac{1}{2}}$ a maximum. Figure 16 gives the dependence of $(R - 1)\ell^{\frac{1}{2}}$ on ℓ for various values of $\bar{k}$. The optimum thickness is seen to be approximately 100A. Figure 17 shows the results of calculations to determine $(R - 1)$ using Eq. (48) and source thicknesses in the neighborhood of the optimum value.

Corrections to be Applied to the Measured Pulse Height

It is desirable to consider the corrections which must be applied to the observed pulse heights prior to a description of the actual measurements. These corrections arise from the fact that the experimental conditions are not exactly the same for the two turntable positions. Consideration is given here to the gain of the electron-detector system for position 1 relative to the gain for position 2. In addition, the effect of a change of the fragment emergence angle with position of the

Fig. 16.--Values of $(R - 1)\ell^{\frac{1}{2}}$ as a function of the total slant thickness for various values of k.

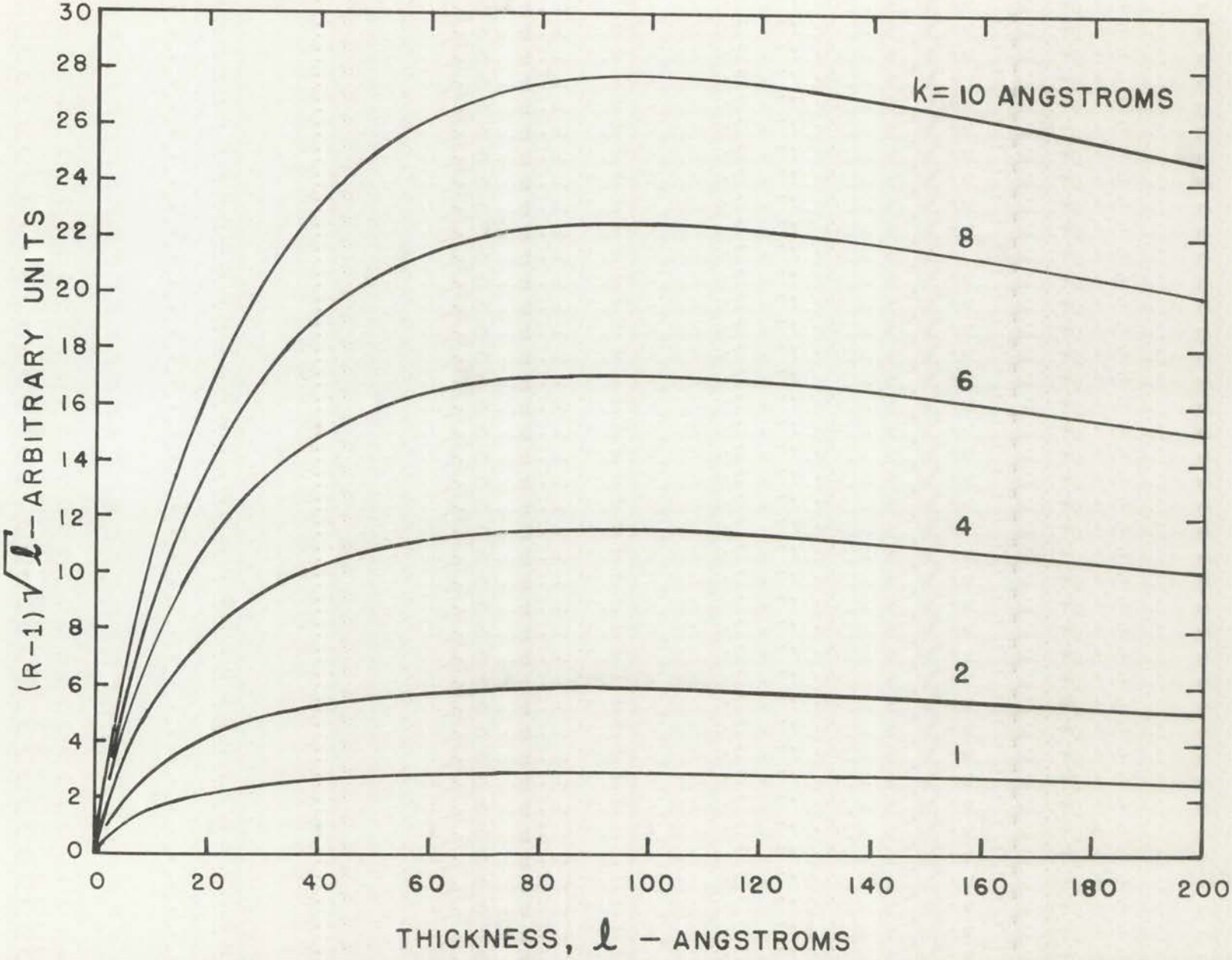
k= 10 ANGSTROMS
8
6
4
2
1
(R-1)√l – ARBITRARY UNITS
THICKNESS, l – ANGSTROMS
0
2
4
6
8
10
12
14
16
18
20
22
24
26
28
30
0
20
40
60
80
100
120
140
160
180
200

Fig. 17.--Values of (R - 1) as a function of k for various values of the total slant thickness.

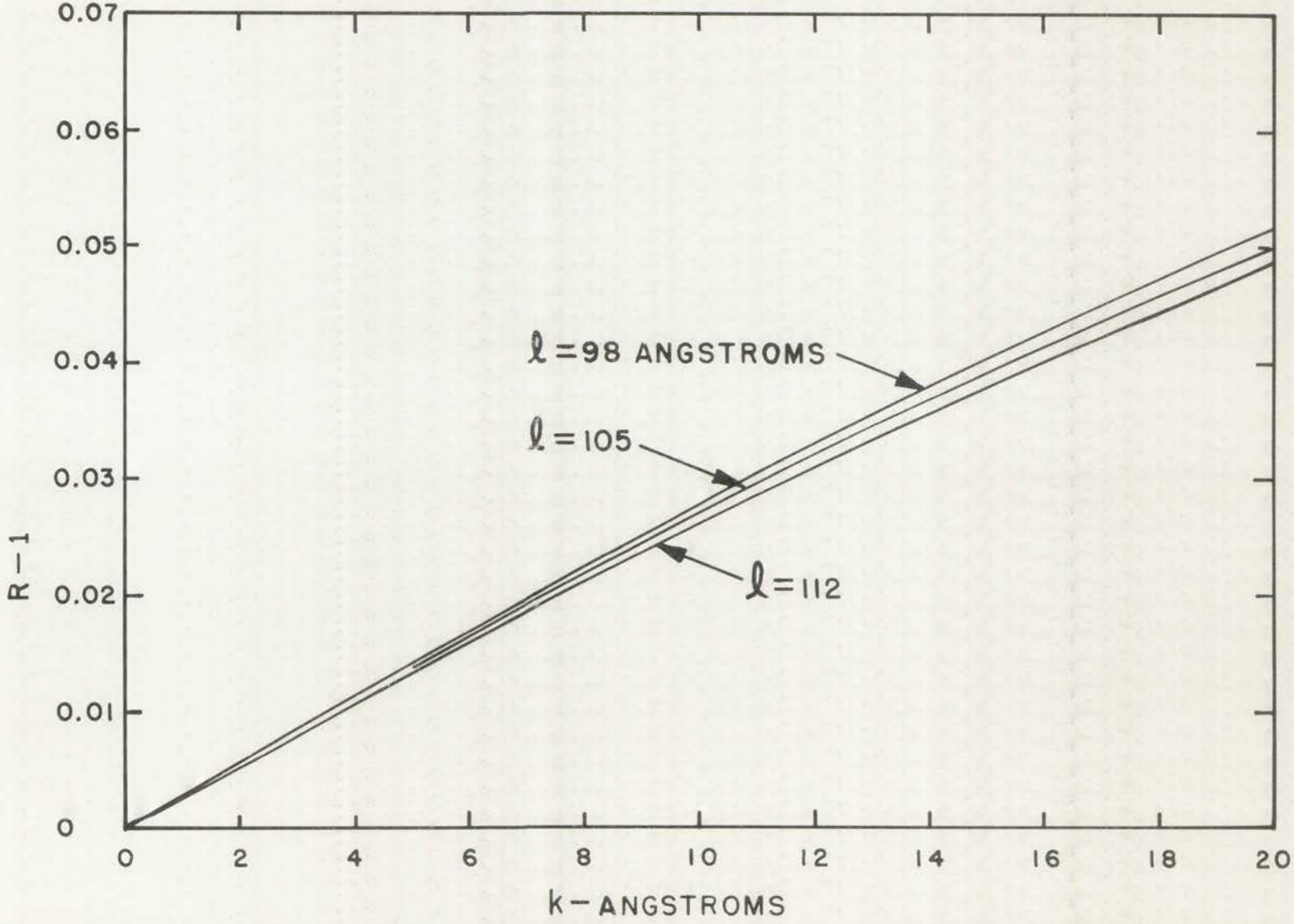
0.07
0.06
0.05
0.04
0.03
0.02
0.01
0
R − 1
0
2
4
6
8
10
12
14
16
18
20
k − ANGSTROMS
ℓ = 98 ANGSTROMS
ℓ = 105
ℓ = 112

turntable is discussed.

Relative Gain Correction

The possibility exists that, with the turntable at position 1, the over-all gain of the electron-detector system is different from the corresponding gain for position 2. To test this possibility and to obtain the proper correction factor, if needed, the gain in position 1 was measured relative to that of position 2. This was accomplished by observing the electron-pulse-height distributions obtained with californium fragments. At regular intervals during the data collection period, the californium source was moved to the "in" position and distributions were obtained for californium fragments with the turntable at each of the two positions. In this arrangement, all except a small fraction of the fragments resulting from neutron-induced fissions were prevented from reaching the top fragment detector by the californium source holder. Therefore, it was not necessary to interrupt the neutron beam or to make any other changes which might have affected the gain stability of the electron-detector system during these measurements. The relative gain is defined by

$$\rho = (C_{H1} + C_{L1})/(C_{H2} + C_{L2}) , \qquad (51)$$

where, again, C_H and C_L refer to the average electron pulse height for the heavy and light californium fragments and the numerical subscripts refer to the two turntable positions. This reduces to $\rho = C_1/C_2$, where C is the average of C_H and C_L taken with equal weighting factors.

Correction for the Emergence Angle

The average-electron-pulse height is expected to be dependent on the emergence angle of the fission fragment. A similar dependence has been observed in the case of secondary electron emission where the experimental results show that the yield of secondary electrons is a function of the angle of incidence of the primary electrons.[26] If, in the present measurements, the emergence angle and, therefore, the observed pulse height with the turntable at position 1 are different from the corresponding quantities at position 2, an erroneous value of R will be observed. Those errors caused by a possible misalignment of the lens or source are not included in the present discussion. Compensation of these errors is automatically included in the relative gain correction given above. Only those effects introduced during the fast-neutron-induced-fission measurements which are not present during the californium measurements are of interest here.

The finite recoil momentum of the compound nucleus can, under certain conditions, cause the emergence angle of the fragments to depend on the turntable position for which a compensation would not be included in the relative gain correction. An evaluation of this correction requires, first, estimates of the average emergence angles for the two turntable positions, and, second, a measurement of the dependence of the average-electron-pulse height on this angle.

Figure 18 illustrates the relationship between the source and fragment detectors in the present experiment. Let the center of the source be the origin, O', of a rectangular corrdinate system with axes x', y' and z'. Here y' and z' represent the directions of the neutron beam and the

Fig. 18.--Schematic diagram of the effective areas of the fragment detectors.

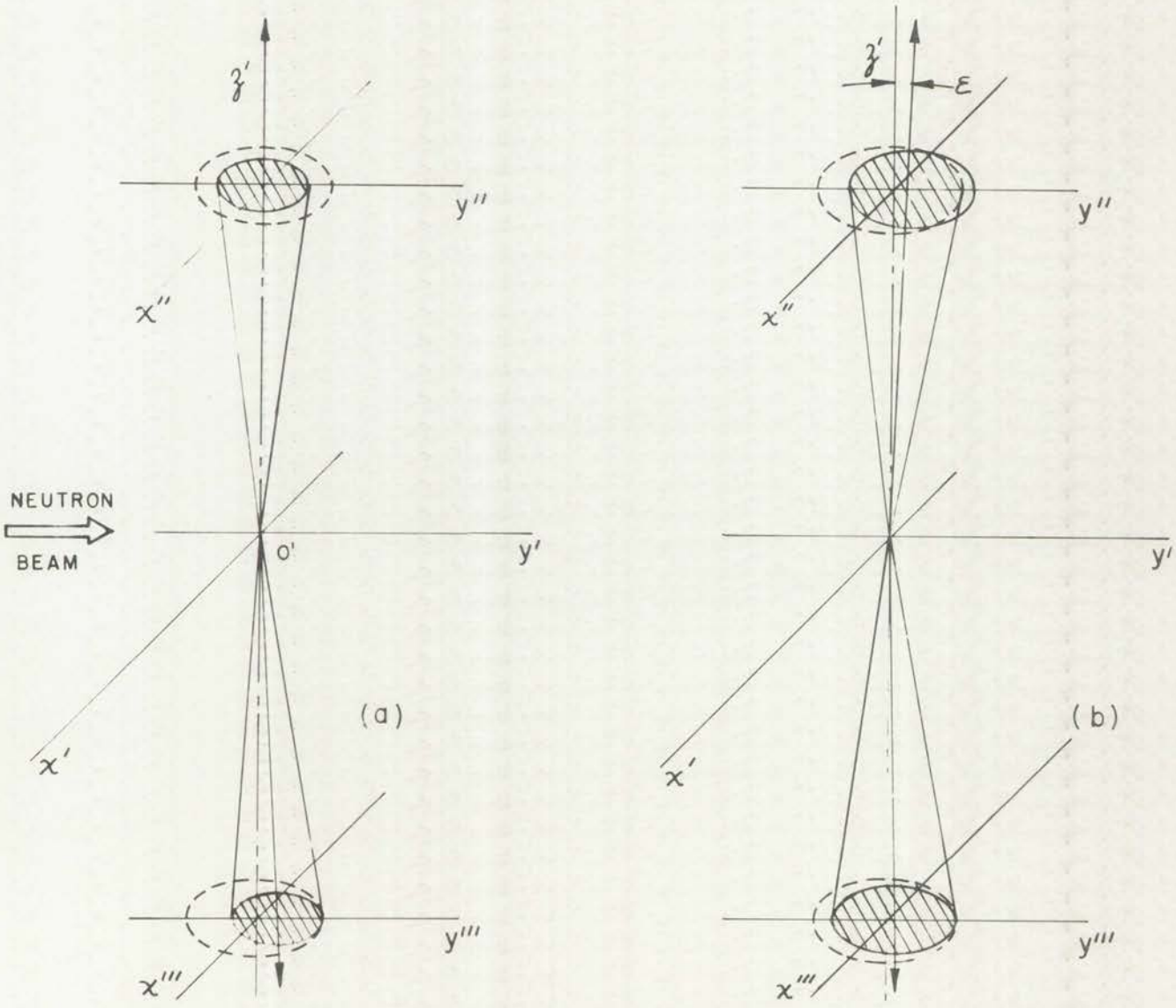
z'
y''
x''
NEUTRON
BEAM
o'
y'
x'
(a)
y'''
x'''
z'
ε
y''
x''
y'
x'
(b)
y'''
x'''

upward vertical, respectively. The upper fragment detector is located in the x" y" - plane with its center at the origin, 0", of the x"y"z' - system. Similarly, the lower fragment detector is located in the x'" y'"- plane with its center at the origin, 0'", of the x'"y'"z'-system. The axes y', y" and y'" are assumed to be parallel and the origins 0" and 0'" are located at z' = D and z' = -D, respectively. Maximum apertures of the fragment detectors are indicated by the ellipses drawn with broken lines.

Angular distributions of the fission fragments have been measured by Simmons and Henkel.[27] These results indicate that the number of fragments emitted per unit solid angle at 90 degrees with respect to the direction of the neutron beam is practically uniform. Therefore, in the following, an isotropic distribution will be assumed. The discussion will be restricted to those fission events for which both fragments are detected. Each fission event may be specified by a point on the x"y" - plane. This is the point of entry into the top detector of the upward-going fragment. The average value of the y"-coordinates depends not only on the velocity of the compound nucleus but also on the apertures of the fragment detectors and the position of the element of source area under consideration. The angle between the directions of the fragment pairs in the laboratory system is less than 180 degrees and will be indicated by $\pi - \beta$. From the known fragment velocities, $v_L = 1.4 \times 10^9$ cm/sec and $v_H = 0.96 \times 10^9$ cm/sec, and the velocity of the center of mass, $v_c = 10^7$ cm/sec, β is found to be 0.017 radians or about one degree. Thus, a fragment entering the center of the lower detector, 0'", is accompanied by its complimentary fragment with position coordinates

$x'' = 0$ and $y'' = 0.53$ cm at the upper detector.

The emergence angle, ψ, is defined as the angle between the foil normal and the fragment direction. The average emergence angle, $\bar{\psi}$, for a given element of source area is defined as the average over all possible values of ψ which are consistent with the restriction that both fragments are detected. The over-all average, $\langle\bar{\psi}\rangle$, is defined as the average of $\bar{\psi}$ over the entire source.

Since the value of $\langle\bar{\psi}\rangle$ is desired only for the evaluation of a correction factor, an estimate of this average angle will be sufficient for the present requirements. For this estimate, let r and θ be the polar coordinates of an element of area dA in the plane of the source. Here, r is measured from the origin, O', and θ is measured from the line defined by the projection of the positive y'-axis on the source plane. The rectangular coordinates of an element of source area described by the polar coordinates r and θ are given by $x' = r\sin\theta$, $y' = (r\cos\theta)/2^{\frac{1}{2}}$, and $z' = \pm(r\cos\theta)/2^{\frac{1}{2}}$, where the plus and minus signs are for position 1 and position 2 of the turntable, respectively. Assume the point where the fragment enters the top detector has coordinates x" and y". The direction cosines of the fragment path are given by: $\alpha_{x'} = (x'' - r\sin\theta)/D'$, $\alpha_{y'} = [y'' - (r\cos\theta)/2^{\frac{1}{2}}]/D'$, and $\alpha_{z'} = [D \mp (r\cos\theta)/2^{\frac{1}{2}}]/D'$, where D' is the distance between the points (x',y',z') and (x'',y'',D). The direction cosines of the normal to the source are: $\beta_{x'} = 0$, $\beta_{y'} = \mp 1/2^{\frac{1}{2}}$, and $\beta_{z'} = 1/2^{\frac{1}{2}}$. The relationship between the angle, ψ, and the direction cosines is expressed by the equation

$$\cos\psi = \alpha_{x'}\beta_{x'} + \alpha_{y'}\beta_{y'} + \alpha_{z'}\beta_{z'} \qquad (52)$$

and the distance, D', is given by the expression

$$D' = [(D \mp z')^2 + (x'' - x')^2 + (y'' - y')^2]^{\frac{1}{2}} . \qquad (53)$$

For this estimate of $\langle\bar{\psi}\rangle$, the above equations will be expanded in powers of r/D, and terms higher than the first order will be neglected. With this approximation, Eq. (53) is given by

$$D' \approx D[1 \mp (r\cos\theta)/2^{\frac{1}{2}}D] \tag{54}$$

and Eq. (52) becomes

$$\cos\psi \approx (1/2^{\frac{1}{2}}) \{\mp y''/D + 1 \pm [(r\cos\theta)/2^{\frac{1}{2}}D]\} \tag{55}$$

Let $\psi = \pi/2 + \epsilon$. For the present conditions, ϵ is of the order of r_o/D, where r_o is the radius of the source. To first order, $\cos\psi \approx (1 - \epsilon)2^{\frac{1}{2}}$. Consequently, $\epsilon \approx \pm y''/D \mp (r\cos\theta)/2^{\frac{1}{2}}D$. The average emergence angle for fragments originating in the element of source area dA with coordinates r and θ is

$$\bar{\psi} = \pi/2 + \bar{\epsilon} , \tag{56}$$

where $\bar{\epsilon} = \pm \overline{y''}(r,\theta)/D \mp (r\cos\theta)/2^{\frac{1}{2}}D$.

Here, $\overline{y''}(r,\theta)$ is the y"-coordinate of the centroid of the cross-hatched area shown in Fig. 18b. To first order, this is the area common to two circles each with radius r_d, where r_d is the radius of each of the fragment detectors. Because of the complicated geometry involved, the actual computation of $\langle\bar{\psi}\rangle$ was not attempted. Instead, an alternative method was used which provided an answer with sufficient accuracy for the present purpose. The values of $\bar{\epsilon}$ were determined for various elements of source area and were found to range from a minimum of about zero to a maximum of one degree. A value of $\langle\bar{\epsilon}\rangle = \pm(0.5 \pm 0.25)^\circ$ was chosen as a reasonable estimate of this angle and its error. Figure 19 illustrates the relationship between $\langle\bar{\psi}\rangle$ and $\langle\bar{\epsilon}\rangle$ for the two turntable positions.

An auxiliary measurement of the average-electron-pulse height

Fig. 19.--Schematic representation of the average emergence angle for the two turntable positions.

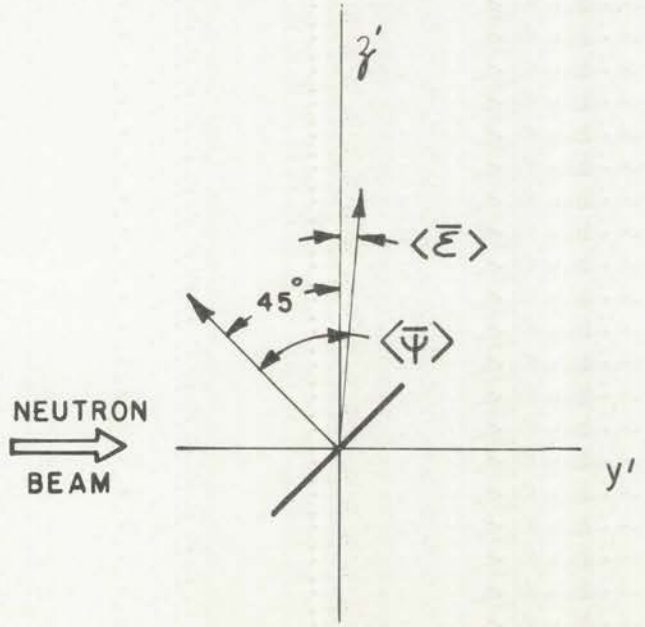

POSITION 1

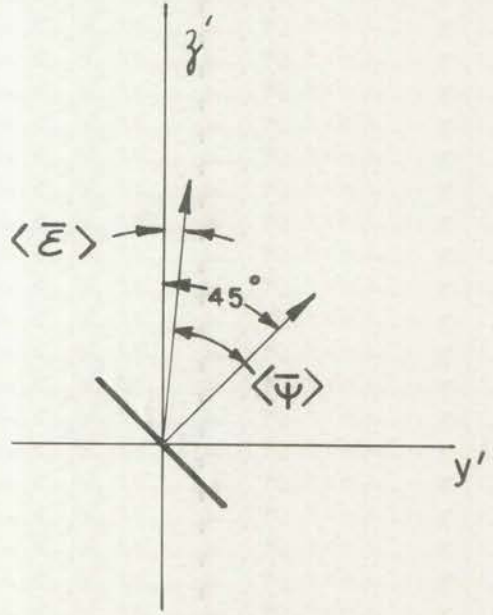

POSITION 2

versus the emergence angle was required to obtain the final correction to be applied to the experimental results. For this measurement, source #14 was used. Here, the fragments originated from the fission of uranium-235 induced by slow neutrons and were, therefore, colinear. With this source, the fission rate was sufficient to provide an adequate counting rate with the area of the lower fragment detector reduced to approximately one-fourth of its normal value. Two separate measurements were required. First, a mask with a two-inch diameter hole in the center was placed over the bottom fragment detector as shown in Figs. 20a and 20b. In this manner, the measurements were restricted to those fragments which emerged vertically within a solid angle defined by the circular hole in the mask. The average emergence angle was 45° for both position 1 and position 2. This measurement was required to determine the average pulse height at position 1 relative to that at position 2 for the same emergence angle.

The average-electron-pulse heights obtained in this measurement are denoted by η' with subscripts H, L, 1 and 2 to indicate the heavy and light fragments and the two turntable positions. These data are shown in Fig. 21, where the values without alphabetic subscripts refer to the average of the corresponding light- and heavy-fragment values.

For the second measurement, another mask with a two-inch diameter hole was used. This mask was placed over the lower detector so that the vertical axis intersected the plane of the mask at the circumference of the hole as shown in Figs. 20c and 20d. For the turntable in positions 1 and 2, the average emergence angles were $\theta_1 = 40.4$ degrees and $\theta_2 = 49.6$ degrees, respectively. The average-electron-pulse heights are

Fig. 20.--Schematic representation of the fragment detector apertures used in the measurements of the average pulse height as a function of emergence angle.

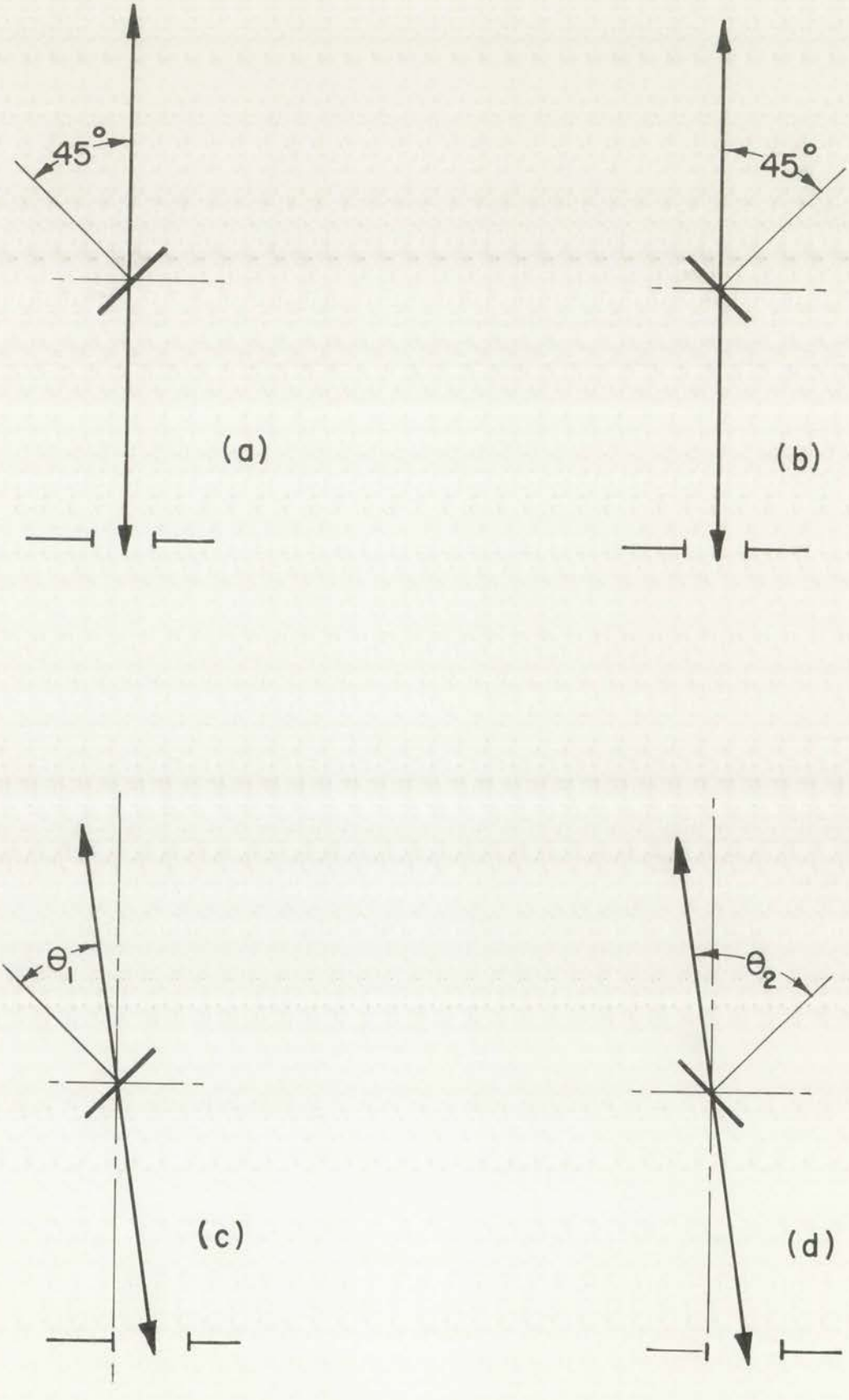
45°
(a)
45°
(b)
θ1
(c)
θ2
(d)

Fig. 21.--Average pulse height as a function of emergence angle.

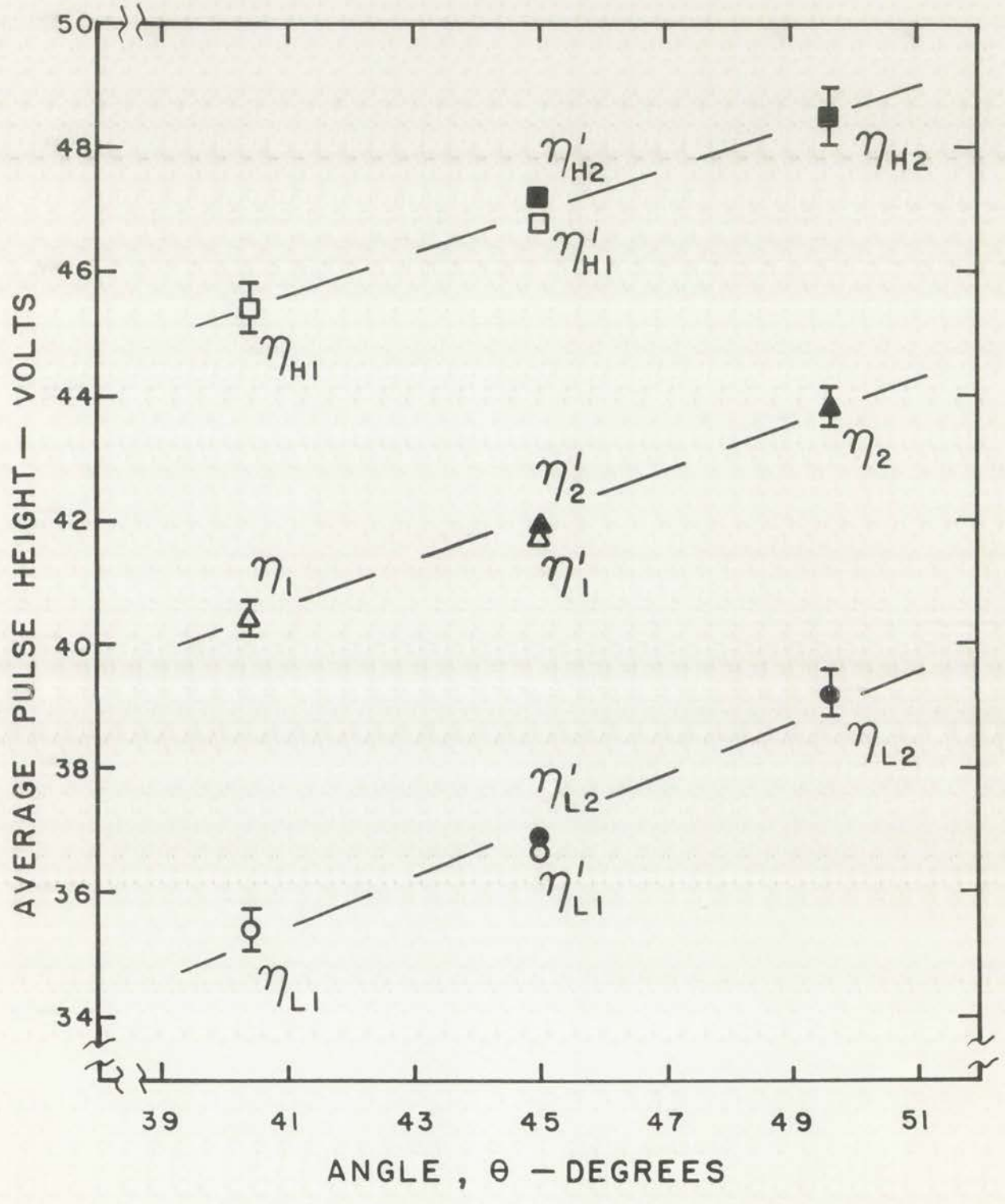
50
48
46
44
42
40
38
36
34
AVERAGE PULSE HEIGHT— VOLTS
η'_{H2}
η_{H2}
η'_{H1}
η_{H1}
η_2
η'_2
η_1
η'_1
η_{L2}
η'_{L2}
η'_{L1}
η_{L1}
39
41
43
45
47
49
51
ANGLE , θ — DEGREES

denoted by η with subscripts similar to those given above. These results are shown in Fig. 21. Standard statistical errors are shown with these data. The errors for the η' results (not shown) are comparable to the errors shown for the η values.

Since the corresponding η' results for the two turntable positions were within the statistical errors, no pulse height corrections were required for the η results. The angular dependence of the average pulse height was represented by the linear function $\eta_i(\theta)=a_i+b_i\theta$, where the subscript i indicated either H or L. In terms of the measured pulse heights, $\eta_i(\theta) = \eta_{io} + (\eta_{i2} - \eta_{i1})(\theta - \theta_o)/(\theta_2 - \theta_1)$, where $\eta_{io} = (\eta_{i2} + \eta_{i1})/2$ and $\theta_o = 45$ degrees. The constant, γ_i, defined by $\gamma_i = \eta_{io}/\eta_i(\theta)$, is the correction factor which when multiplied by a pulse height measured at an emergence angle, θ, gives the corrected pulse height for $\theta = \theta_o$. This factor is given by

$$\gamma_i = \eta_{io}/[\eta_{io} + (\lambda_i/\Delta)(\theta - \theta_o)] , \tag{57}$$

where $\lambda_i = \eta_{i2} - \eta_{i1}$ and $\Delta = (\theta_2 - \theta_1)$. Since λ_i is small compared to η_{io} and $(\theta - \theta_o)$ is small compared to Δ,

$$\gamma_i \approx 1 - (\lambda_i/\eta_{io})(\theta - \theta_o)/\Delta . \tag{58}$$

From the above discussion, the average emergence angle was $\langle\bar{\psi}\rangle_1 = 45^o + |\langle\bar{\epsilon}\rangle|$ for position 1 and $\langle\bar{\psi}\rangle_2 = 45^o - |\langle\bar{\epsilon}\rangle|$ for position 2. Therefore, the correction factors to be used with the fast-neutron data are

$$\gamma_{i1} = 1 - \lambda_i|\langle\bar{\epsilon}\rangle|/\eta_{io}\Delta \tag{59}$$

and

$$\gamma_{i2} = 1 + \lambda_i|\langle\bar{\epsilon}\rangle|/\eta_{io}\Delta \tag{60}$$

These are the estimated corrections to be applied to the average electron-pulse heights when fragment detectors with equal apertures are used. If, however, the fission rate is sufficient to provide reasonable counting rates with the top detector masked as shown in Fig. 18a, no corrections are required. In the present experiment, data were obtained under both conditions.

Application of the Present Method

Procedure

Measurements were performed to determine the pulse-height ratios, R, for sources of U-238 and Np-237. These nuclei were chosen for the following reasons: First, each has a characteristic neutron energy below which neutron-induced fission is very improbable. Thus, only neutrons with energies above this threshold are effective in these measurements. This establishes a lower limit for the recoil velocities and, therefore, precludes the possibility of a contribution to $\langle\bar{\xi}(E)\rangle_1$ and $\langle\bar{\xi}(E)\rangle_2$ for values of E less than the threshold energy. Such a contribution would cause the ratio, R, to approach unity and make this experiment more difficult. Second, these isotopes were available with high purity. Contaminants which undergo slow-neutron-induced fission would be undesirable for the same reason given immediately above. The U-238 sample used in these measurements had a U-235 impurity of 11 PPM and the Np-237 sample contained approximately 20 PPM of plutonium. Since both contaminants have cross sections for slow-neutron-induced fission which are approximately 10^3 times the fast-neutron cross sections of either U-238 or Np-237, these impurities contribute

only one or two percent to the total fission rate.

One U-238 and two Np-237 sources with thicknesses of 112A, 98A and 105A, respectively, were prepared using the standard procedure given in Appendix A. The thicknesses were determined from the emission rates of natural alpha particles and the known specific activities. The data-collection rate for the U-238 source was about one fission event per minute and the Np-237 rate was approximately four events per minute. These counting rates were applicable to the experimental arrangement indicated in Fig. 18b. This arrangement was used for the U-238 and the first Np-237 source. For the remaining neptunium foil, the aperture of the top fragment detector was restricted to a diameter of 3.3 inches, which insured that the average emergence angle, $\langle \bar{\psi} \rangle$, was the same for the two turntable positions.

The procedure for these measurements was as follows: One of the sources was mounted on the central lens element and the vacuum chamber was evacuated as rapidly as possible. The cold trap was then cooled with liquid nitrogen. As soon as the pressure within the vacuum chamber reached a value close to the ultimate vacuum ($\sim 10^{-6}$ mm of Hg), the lens voltage was applied and the neutron beam was turned on. A period of approximately four hours was required for the stabilization of the gain of the photomultiplier associated with the electron detector. Measurements were then made of the electron-pulse-height distributions for californium fragments entering the source with the turntable in both positions. For these measurements, the turntable was rotated every twenty minutes and data were obtained for at least nine twenty-minute periods. With the californium source, the counting rate was about 40 fission events per minute. The data obtained during the

odd numbered counting periods, when the turntable was in position 1, were identified by an odd identification number. Even identification numbers were assigned to those data obtained during the even numbered counting periods, when the turntable was in position 2. Hereafter, the data obtained during each counting period will be called a "record". The californium source was moved to the "out" position and similar data were obtained for fast-neutron-induced fissions. For these measurements, the turntable was rotated every hour and the total counting time was approximately 20 hours. This constituted one "run" and a series of these runs, each beginning with californium data, comprised the measurement for a particular source.

From the californium data, the relative gain, ρ_r, and its statistical error, $\sigma(\rho)_r$, were computed for each run. From the neutron-induced-fission data the value of the observed ratio of the pulse heights, R'_r, and its statistical error, $\sigma(R')_r$, were also obtained for each run. The details of these computations are given in Appendix C. The final observed ratio for a given measurement was obtained from a weighted average of the individual R'_r values and is given by

$$R' = \sum_r w(R')_r R'_r / \sum_r w(R')_r , \tag{61}$$

where r takes on integer values from one up to, and including, the number of runs. The value of the final relative gain is given by

$$\rho = \sum_r w(\rho)_r \rho_r / \sum_r w(\rho)_r , \tag{62}$$

where the summations are over the number of californium runs contained in the measurement. In the above, the weighting factors, w, were obtained as usual from the inverse of the variance, $w = 1/\sigma^2$. The final corrected

ratio is given by

$$R = R'/\rho. \tag{63}$$

The statistical errors were obtained from the following relationships:

$$\sigma^2(R') = 1/\sum_r w(R')_r, \tag{64}$$

$$\sigma^2(\rho) = 1/\sum_r w(\rho)_r, \tag{65}$$

and $$\sigma^2(R)/R^2 = \sigma^2(R')/(R')^2 + \sigma^2(\rho)/\rho^2 . \tag{66}$$

The relationship between the ratio, R, and the average recoil distance, $\bar{k}$, is given by a substitution of the expressions in Eq. (46) and (47) into Eq. (48). This function is plotted in Fig. 17 for the deposit thicknesses which were used in the present experiment. In the region of interest, where $\bar{k}$ is less than 10A, these curves show that the expressions given in Eq. (49) or (50) can be used with negligible error. Thus

$$\bar{k} = \alpha(R - 1),$$

where α is determined either from these equations or from the curves in Fig. 17. From the definition of $\bar{k}$ given immediately after Eq. (46), the measured mean lifetime is

$$\tau(\bar{E}) = \alpha(R - 1)/\hat{v}_c \tag{67}$$

and the statistical error is

$$\sigma(\tau) = (\alpha/\hat{v}_c)\sigma(R) . \tag{68}$$

The effective velocity of the compound nucleus, $\hat{v}_c$, was defined by

$\hat{v}_c = (2m\bar{E})^{\frac{1}{2}}/(M + m)$, where $\bar{E}$ is the average energy of those neutrons which are effective in this experiment.

Uranium-238 Source

The conditions for the U-238 source were as follows:

Deposit thickness = 112A

$\gamma_{H1} = 0.9964$

$\gamma_{L1} = 0.9945$

$\gamma_{H2} = 1.0036$

$\gamma_{L2} = 1.0055$

$\alpha = 3.77 \times 10^{-6}$ cm

$\bar{E} = 2.8$ Mev

$\hat{v}_c = 0.97 \times 10^{7}$ cm/sec.

The results obtained with this source are given in Table 6.

TABLE 6

RESULTS FOR THE URANIUM-238 SOURCE

Run Number r	R'_r	$\sigma^2(R')_r$	ρ_r	$\sigma^2(\rho)_r$
1	0.980	1.69×10^{-4}	1.016	2.41×10^{-4}
2	0.99	1.67×10^{-4}	1.008	0.81×10^{-4}
3	1.007	1.51×10^{-4}	1.005	0.84×10^{-4}

The average corrected ratio was $R = 0.987 \pm 0.009$ and the mean lifetime was found to be $\tau = (-5 \pm 4) \times 10^{-15}$ sec.

First Neptunium-237 Source

The conditions for this source were as follows:

Deposit thickness = 98A

$\gamma_{H1} = 0.9964$

$\gamma_{L1} = 0.9945$

$\gamma_{H2} = 1.0036$

$\gamma_{L2} = 1.0055$

$\alpha = 3.49 \times 10^{-6}$ cm

$\bar{E} = 2.2$ Mev

$\hat{v}_c = 0.87 \times 10^{7}$ cm/sec.

The results obtained with this source are given in Table 7.

TABLE 7

RESULTS FOR THE FIRST NEPTUNIUM-237 SOURCE

Run Number r	R'_r	$\sigma^2(R')_r$	ρ_r	$\sigma^2(\rho)_r$
1	1.016	0.56×10^{-4}	1.006	1.63×10^{-4}
2	0.990	0.60×10^{-4}	1.013	1.97×10^{-4}
3	1.004	0.58×10^{-4}	1.007	1.03×10^{-4}
4	1.014	0.69×10^{-4}	1.002	1.86×10^{-4}
5[a]			0.991	1.36×10^{-4}
6[a]			1.022	1.28×10^{-4}
7[a]			1.003	1.78×10^{-4}

[a]Three additional californium runs were made during this measurement.

The average corrected ratio was $R = 0.999 \pm 0.006$ and the mean lifetime was $\tau = (-0.2 \pm 2.5) \times 10^{-15}$ sec.

Second Neptunium-237 Source

The conditions for this source were as follows:

Deposit thickness = 105A

Top fragment detector was 3.3-inch diam, therefore, all gammas were equal to unity

$\alpha = 3.62 \times 10^{-6}$ cm

$\bar{E} = 2.2$ Mev

$\hat{v}_c = 0.87 \times 10^{7}$ cm/sec

The results obtained with this source are given in Table 8.

TABLE 8

RESULTS FOR THE SECOND NEPTUNIUM-237 SOURCE

Run Number r	R'_r	$\sigma^2(R')_r$	ρ_r	$\sigma^2(\rho)_r$
1	0.996	1.48×10^{-4}	1.005	1.21×10^{-4}
2	1.019	1.35×10^{-4}	0.991	1.19×10^{-4}
3	1.012	8.66×10^{-4}	1.002	1.18×10^{-4}
4	1.004	1.86×10^{-4}	1.022	1.35×10^{-4}
5	1.006	1.32×10^{-4}	0.997	1.26×10^{-4}
6	0.983	1.40×10^{-4}	0.999	1.36×10^{-4}
7	1.015	1.77×10^{-4}	1.017	1.31×10^{-4}
8	0.994	1.38×10^{-4}	1.013	1.52×10^{-4}

The average corrected ratio was $R = 0.997 \pm 0.006$ and the mean lifetime was $\tau = (-1.2 \pm 2.6) \times 10^{-15}$ sec.

Negative values of the mean lifetime, of course, have no physical significance. They are caused by statistical and possible systematic errors in the measurements. The values of τ obtained from this experiment are all consistent with a zero mean lifetime of the compound nucleus.

Change of the Source Characteristics

The calibration data described in Chapter IV apply strictly to a source which had been in the vacuum chamber for approximately one day, whereas, the mean lifetime measurements considered in this chapter required one to two weeks to complete. The possibility exists that the surface of the source may have changed during this longer irradiation time in such a way as to require a calibration different from the one obtained in Chapter IV. If, for example, oil vapors condensed on the fissile layer thereby creating an inert layer on top of the fissile deposit, the sensitivity of this method would have been decreased. Only changes which occurred after about one day are of interest in the present discussion. This was the approximate time required to obtain the data from each of the calibration sources. The effects of any change of the surface characteristics which occurred prior to this time are assumed to be present not only in the calibration data but also in the mean-lifetime results as well.

This hypothesis was tested by means of an auxiliary measurement. For this determination, foil #10 was mounted in the vacuum system for the first time. (The data reported previously in Chapter IV for source #10 were obtained during this measurement.) Electron-pulse-height

distributions were obtained for both californium and U-235 fragments at various times during a period of one week. The experimental conditions were similar to those which were used for the mean-lifetime measurements. A calculation similar to the one employed to obtain Eq. (46) indicates that the relative pulse height will be an increasing function of the thickness of this proposed inert layer.

The results of this measurement are given in Table 9.

TABLE 9

RESULTS OF THE AUXILIARY MEASUREMENT

Time after Installation of the Source (Days)	Relative Pulse Height U/C
1	1.30 ± 0.01
2	1.31 ± 0.01
6	1.29 ± 0.01
7	1.31 ± 0.01

No significant change of the relative pulse height was observed for this source. It is, therefore, unlikely that a deposit of oil vapor reduced measurably the sensitivity of the measurements of the mean lifetimes.

Conclusions

These results show that, within the sensitivity of the present method, the mean lifetimes of the compound nuclei studied are consistent with zero. However, an upper limit of this lifetime, which is

many orders of magnitude below those obtained previously by other methods, can be determined from these results. Estimates of these upper limits require a detailed investigation of the error involved in the present measurements.

The approximate expression for the mean lifetime given by Eq. (67)

$$\tau = (\alpha/\hat{\nu}_c)\ (R - 1)$$

will be adequate for the following discussion. Since the errors associated with α, $\hat{\nu}_c$ and R are independent, the uncertainty of the mean lifetime is

$$\sigma^2(\tau) = (\alpha/\hat{\nu}_c)^2\ \sigma^2(R) + [\alpha(R - 1)/\hat{\nu}_c^{\,2}]^2\sigma^2(\hat{\nu}_c)$$

$$+ [(R - 1)/\hat{\nu}_c]^2\sigma^2(\alpha)\ . \qquad (69)$$

For the conditions of this experiment, where R is practically unity, this expression becomes

$$\sigma(\tau) \approx (\alpha/\hat{\nu}_c)\ \sigma(R)\ . \qquad (70)$$

In addition to the statistical uncertainties, which have been given for each measurement, the total error of R also includes the uncertainty associated with the values of the correction terms γ_{i1} and γ_{i2}. From the estimate of the angle $< \bar{\epsilon} >$ and the uncertainties associated with the η-values, this additional error is estimated to contribute about 0.5 percent to the total error of R. The final values for the errors of the ratio and mean lifetimes are as follows: For U-238, $\sigma(R) = 0.01$ and $\sigma(\tau) = 4 \times 10^{-15}$ sec and, for Np-237, $\sigma(R) = 0.008$

and $\sigma(\tau) = 3.5 \times 10^{-15}$ sec.

Upper limits for the mean lifetimes, τ_u, were estimated using the method of tolerance limits described by Bowker in the compilation edited by Eisenhart et al.[28] It was assumed that the values of τ for each run were independent samples from a normal distribution with mean equal to zero and variance $\sigma^2(\tau_r)$. Here, $\sigma^2(\tau_r)$ is the variance of the mean lifetime for each run and was taken to be the product of the number of runs, n_r, and the variance of the average τ obtained for each source, i.e., $\sigma^2(\tau_r) = n_r\, \sigma^2(\tau)$ which is the usual relationship between the variance of the distribution and the variance of the mean. The upper tolerance limit is given by $\tau_u = \tau + k\sigma(\tau_r)$. Here, k is a standard statistical notation for the multiple of the standard deviation and has no relationship to the k used previously. Values of k were obtained from the tables for one-sided tolerance limits given by D. B. Owen[29] and were chosen such that at least 97.5 percent of the normal population was less than $\tau_u = k\sigma(\tau_r)$ with a 95-percent confidence. The values of k for the number of runs or samples for each measurement were as follows:

$$n_r = 3; \quad k = 8.986$$

$$n_r = 4; \quad k = 6.015$$

$$n_r = 8; \quad k = 3.723$$

From the previous estimates of the mean-lifetime errors, the number of runs for each measurement, and the appropriate value of k, the total mean lifetimes were found to be $\tau(\text{U-238}) < 6 \times 10^{-14}$ sec and $\tau(\text{Np-237}) < 4 \times 10^{-14}$ sec.

Estimates of the partial mean lifetimes for neutron emission,

τ_n, and fission, τ_f, were obtained from the relationship $\Gamma = \Gamma_n + \Gamma_f$. Since each width is proportional to the reciprocal of the corresponding mean lifetime, $1/\tau = 1/\tau_n + 1/\tau_f$. Therefore, the solutions for the partial mean lifetimes, in terms of the ratio of the neutron width to the fission width and the total mean lifetime, are $\tau_f = \tau\ (1 + \Gamma_n/\Gamma_f)$ and $\tau_n = \tau\ (1 + \Gamma_f/\Gamma_n)$. From cross section measurements, Vandenbosch and Huizenga[30] have obtained the following neutron emission to fission width ratios for 3-Mev neutrons: Γ_n/Γ_f(U-238) = 5.13 and Γ_n/Γ_f (Np-237) = 1.32. With these values the partial mean lifetimes for U-238 determined from this experiment are $\tau_f < 4 \times 10^{-13}$ sec and $\tau_n < 7 \times 10^{-14}$ sec. The corresponding lifetimes for Np-237 are $\tau_f < 9 \times 10^{-14}$ sec and $\tau_n < 7 \times 10^{-14}$ sec.

The present values of the total mean lifetimes may be compared with the value of τ less than about 10^{-9} sec obtained for U-235 by Wilson.[6] The values from the present work are, therefore, about four orders of magnitude less than this previously reported mean lifetime. The present data are consistent with the result that some fissions occur within 5×10^{-13} sec which was obtained by Feather.[5]

APPENDIX A

SOURCE PREPARATION

The sources used in this experiment were uniform in regard to the support material and holders. They differed only in the amount and type of material deposited. The foil holders consisted of a pair of rings made of 22-gage (1/32-inch) nickel and were held together by eight #0-80 stainless steel screws. Each ring had an inside diameter of 1.75 inches. The outside diameters of the top and bottom rings were 2.25 and 2.75 inches, respectively. Nickel foil of thickness 5×10^{-6} inches was used as the support material. These foils were made by electrodeposition and were supplied[31] with a copper backing approximately 10^{-4} inches thick. The copper backed nickel foil and a 20-mesh, 93-percent transparent nickel screen[32] were clamped together between the two rings. The screen was placed on the nickel side of the foil and the exposed copper was dissolved away by immersing the assembly in a solution of chromic acid. This technique has been previously described by Bashkin and Goldhaber.[33] The nickel foil usually adhered to the reinforcing screen after the copper was dissolved. This provided a stronger foil than would have been obtained in the absence of the screen. Only those foils with plane surfaces were selected for use in this experiment.

Tetrafluoride compounds of the fissile material were deposited on the clear side of the foil by the technique of vacuum evaporation. The deposits were confined to the central region of the foil. This was accomplished by placing a mask with a 1.125-inch diameter hole over the

clear face of the foil during the evaporation of the fissile material. After the evaporation, another mask with a one-inch diameter hole was mounted permanently on the screen side of the foil holder. Sheets of 0.001-inch thick molybdenum were used, although other materials with sufficient thickness to stop fission fragments would have been satisfactory. This mask was required primarily to define the source area during the californium measurements. Only those fragments which entered the source within this one-inch-diameter circle could reach the bottom detector and provide the pulse necessary for a triple coincidence. In this manner, californium data were obtained only for those fragments which entered the fissile deposit. Those fragments which entered the uncovered nickel foil were not observed.

APPENDIX B

APPROXIMATE EVALUATION OF $\langle\bar{\xi}(E)\rangle$

In Chapter V, the average-pulse height for all effective-neutron energies was given by

$$\langle\bar{\xi}(E)\rangle = \int_0^\infty \bar{\xi}(E)\, S(E)\, dE \,, \tag{1B}$$

where for position 1

$$\bar{\xi}(E)_1 = H(0)\left\{A - [Bg^2/\ell(k + g)][1 - \exp(-\ell/g)]\right\} , \tag{2B}$$

for position 2

$$\bar{\xi}(E)_2 = H(0)\left\{A + [Bk^2/\ell(g - k)]\,[1 - \exp(-\ell/k)] - [Bg^2/\ell(g - k)]\,[1 - \exp(-\ell/g)]\right\} , \tag{3B}$$

and

$$k(E) = (2\mu E)^{1/2}\, \tau(E)/(M + \mu) . \tag{4B}$$

For $k \ll g$ and $g < \ell$, Eqs. (2B) and (3B) become

$$\bar{\xi}(E)_1 \approx H(0)\left\{A - (Bg/\ell)[1 - \exp(-\ell/g)] + (Bk/\ell)\,[1 - \exp(-\ell/g)]\right\}$$

or

$$\bar{\xi}(E)_1 \approx a + b'k \tag{5B}$$

and

$$\bar{\xi}(E)_2 \approx H(0)\left\{A - (Bg/\ell)[1 - \exp(-\ell/g)] - (Bk/\ell)[1 - \exp(-\ell/g)]\right\}$$

or

$$\bar{\xi}(E)_2 \approx a - b'k \tag{6B}$$

where

$$a = H(0)\left\{A - (Bg/\ell)\,[1 - \exp(-\ell/g)]\right\}$$

and

$$b' = H(0)\left\{(B/\ell)[1 - \exp(-\ell/g)]\right\} \quad .$$

Therefore, it will be sufficient to consider the one expression

$$\bar{\xi}(E) \approx a + bk$$

where $b = +b'$ for position 1 and $b = -b'$ for position 2. An expression for the fission width $\Gamma_f(E)$ has been obtained by Fujimoto and Yamaguchi[34] which was based on the Fermi gas model of the nucleus. Their result was

$$\Gamma_f \approx T \exp(-E_f/T) , \tag{7B}$$

where the nuclear temperature, T, is given in terms of the excitation energy, E_x, and the constant, a, by

$$T = (E_x/a)^{1/2} .$$

The quantity E_f is the energy of the fission barrier and E_x is the sum of the neutron kinetic energy, E, and the binding energy of the neutron, B_n. From the uncertainty relation

$$\tau_f(E) = K' [a/(E + B_n)]^{1/2} \exp\left\{ E_f [a/(E + B_n)]^{1/2} \right\} ,$$

where K' is an unknown constant of proportionality. If this expression is used as an estimate of the dependence of the mean lifetime on the neutron energy, the pulse height is given by

$$\bar{\xi}(E) \approx a + c\, E^{1/2}\, \Lambda \exp(p\Lambda)$$

where $c = b\,(2u)^{1/2}/(M + m)K'\, a^{1/2}$, $p = E_f a^{1/2}$, and $\Lambda = 1/(E + B_n)^{1/2}$.

From Taylor's formula, $\bar{\xi}(E) = \xi(\bar{E}) + (E - \bar{E})\, \xi'(\bar{E}) + I(E)$, where the remainder

$$I(E) = (E - \bar{E})^2\, \xi''(E_1)/2$$

and the unknown E_1 depends on the value of E. The average of $\bar{\xi}(E)$ is given by the sum of the averages

$$\langle \xi(E) \rangle = \xi(\bar{E}) + \langle I(E) \rangle ,$$

where the second term is zero, since $\langle E - \bar{E} \rangle = 0$.

The error introduced by setting $\langle \bar{\xi}(E) \rangle = \bar{\xi}(\bar{E})$ is obtained in the following manner: Consider the absolute value of the relative error

$$|\text{Rel. error}| = \frac{|\langle I \rangle|}{\xi(\bar{E})}.$$ If for all values of E under consideration $|\xi''(E)| \leq M_\xi$, then

$$|I| \leq M_\xi (E - \bar{E})^2/2 \text{ and } \langle |I| \rangle \leq M_\xi \langle (E - \bar{E})^2 \rangle /2 .$$

Since $|\langle I \rangle| \leq \langle |I| \rangle$, $|\langle I \rangle| \leq M_\xi \langle (E - \bar{E})^2 \rangle / 2$ and

$$|\text{Rel. error}| \leq M_\xi \langle (E - \bar{E})^2 \rangle /2 \, \bar{\xi}(\bar{E}) .$$

The values of $|\xi''(E)|$ were determined for various values of E, and a value of $M_\xi = 0.04 \, \bar{\xi}$ was found to be valid for the energy region considered here. The energy spectra of effective neutrons S(E) are shown in Fig. 22 for the target nuclei used in this experiment. From these curves, it is evident that $\langle (E - \bar{E})^2 \rangle \leq 2.2 \text{ Mev}^2$. Therefore,

$$|\text{Rel. error}| \leq \frac{(0.04\bar{\xi})\,(2.2)}{2\bar{\xi}} \text{ which gives } |\text{Rel. error}| \leq 0.05.$$

Thus, $\langle \bar{\xi}(E) \rangle$ may be set equal to $\bar{\xi}(\bar{E})$ with an error of about five percent.

Fig. 22.--Normalized energy spectra of the neutrons which are effective in the present measurements.

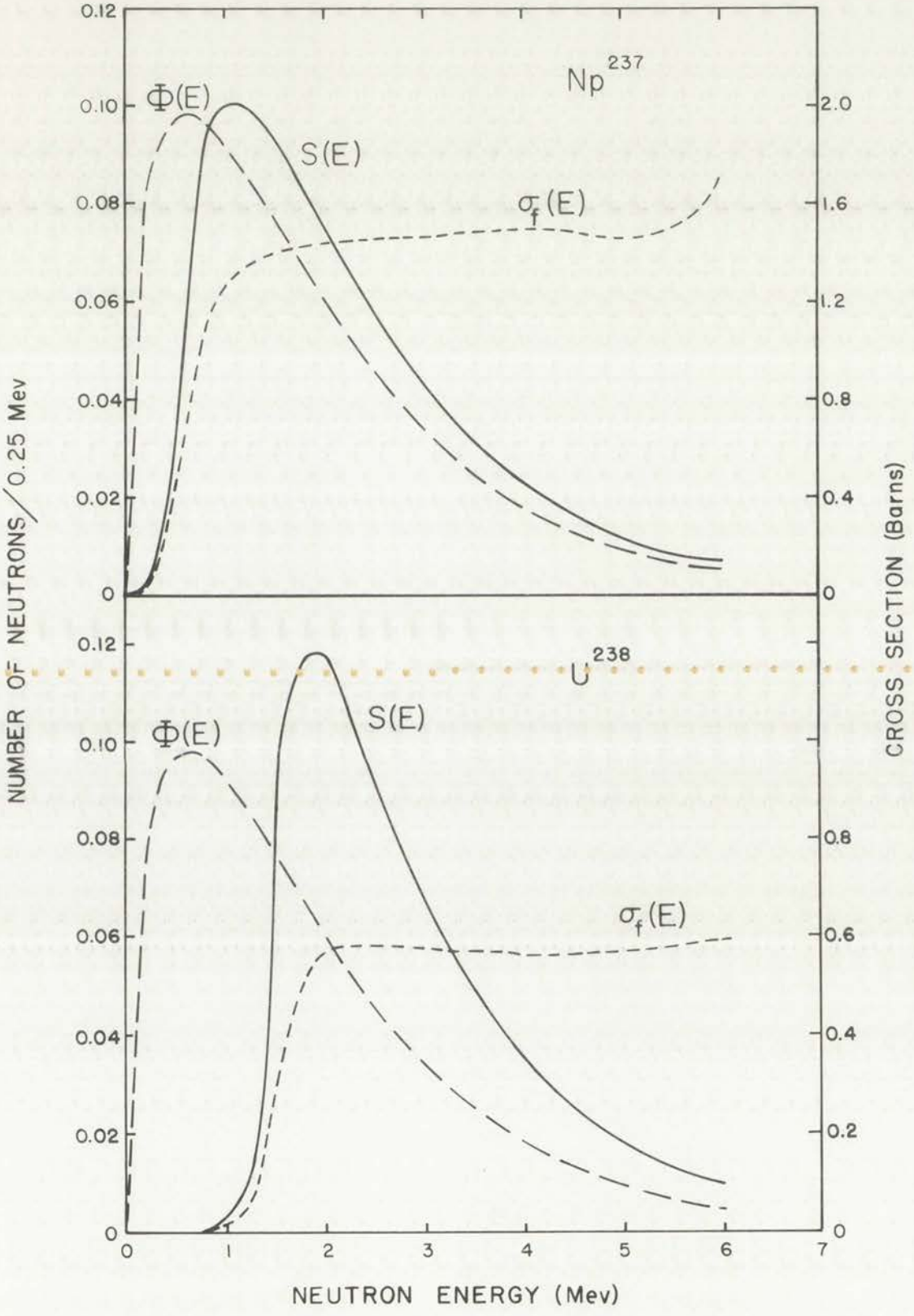
Np 237
Φ(E)
S(E)
σf(E)
U 238
Φ(E)
S(E)
σf(E)
NUMBER OF NEUTRONS / 0.25 Mev
CROSS SECTION (Barns)
NEUTRON ENERGY (Mev)
0.12
0.10
0.08
0.06
0.04
0.02
0
2.0
1.6
1.2
0.8
0.4
0.2
1
2
3
4
5
6
7

APPENDIX C

TREATMENT OF THE EXPERIMENTAL DATA

For each fission event detected, the magnitudes of the pulses occurring at the inputs of channels I and III of the pulse-height analyzer were recorded on punched paper tape. The first three digits (0-199) represented the height of the pulse from the electron detector and the last three digits gave the height of the pulse from the time-to-pulse height converter. These data were transferred to magnetic tape which served as the data-input tape for an IBM 704 Data Processing System. Each event was characterized by the height of the pulse which was analyzed in channel III (see Chapter IV). Those events which correspond to the higher peak of the distribution shown in Fig. 11b were associated with fissions in which the light fragment was emitted in the upward direction. Those events corresponding to the lower peak were associated with fissions in which the light fragment was emitted in the downward direction. Thus, each of the electron pulse heights recorded in channel I was identified with either a light or heavy fragment emerging from or entering the source.

Let the electron pulse height of the j-th event in the w-th record be denoted by ξ_{ijw}, where i indicates the type of fragment, either heavy, H, or light, L. The average pulse height was obtained for each record from the expression

$$\bar{\xi}_{iw} = \sum_{j=1}^{n_{iw}} \xi_{ijw}/n_{iw} \,, \tag{1C}$$

where n_{iw} is the number of events of type i in the w-th record. The average pulse height for the odd records, where the turntable was at position 1, was found from the relation

$$\bar{\xi}_{i1} = \sum_{w=1}^{m_1} \bar{\xi}_{iw}\, n_{iw} / \sum_{w=1}^{m_1} n_{iw} \,, \tag{2C}$$

where $w = 1,3,5\ldots.$, m_1 and m_1 is the number of odd records. The average pulse height for the even records was found from a similar expression,

$$\bar{\xi}_{i2} = \sum_{w=2}^{m_2} \bar{\xi}_{iw}\, n_{iw} / \sum_{w=2}^{m_2} n_{iw} \,, \tag{3C}$$

where $w = 2,4,6\ldots.$, m_2 and m_2 is the number of even records. The corrected average pulse heights were obtained from the relations

$$\bar{\bar{\xi}}_{i1} = \gamma_{i1}\, \bar{\xi}_{i1} \tag{4C}$$

and

$$\bar{\bar{\xi}}_{i2} = \gamma_{i2}\, \bar{\xi}_{i2} \,, \tag{5C}$$

where the gammas were obtained from Eqs. (59) and (60). The average pulse heights for the two turntable positions were obtained from the expressions

$$< \bar{\xi} >_1 = (\bar{\bar{\xi}}_{H1} + \bar{\bar{\xi}}_{L1})/2 \tag{6C}$$

and

$$< \bar{\xi} >_2 = (\bar{\bar{\xi}}_{H2} + \bar{\bar{\xi}}_{L2})/2 \,. \tag{7C}$$

Finally, the observed ratio for all records in the r-th run was given by

$$R'_r = \langle \bar{\xi} \rangle_1 / \langle \bar{\xi} \rangle_2 . \tag{8c}$$

The statistical uncertainties associated with these observed quantities were determined as follows: The mean square of the deviations were computed separately for the heavy- and light-fragment events contained in the entire run. No distinction between even or odd records was made. The average of the square of the pulse heights was given by

$$\overline{\xi_i^2} = \sum_{w=1}^{m} \sum_{j=1}^{n_{iw}} \xi_{ijw}^2 / \sum_{w=1}^{m} n_{iw} , \tag{9c}$$

where $m = m_1 + m_2$. The average pulse height for all events with fragment type i was obtained from

$$\bar{\xi}_i = \sum_{w=1}^{m} \bar{\xi}_{iw} \, n_{iw} / \sum_{w=1}^{m} n_{iw}$$

and the mean square deviation of the observed pulse height distribution for fragments of the type i was given by

$$\sigma^2(\xi_i) = \overline{\xi_i^2} - (\bar{\xi}_i)^2 . \tag{10c}$$

Thus, $\sigma(\xi_H)$ and $\sigma(\xi_L)$ are the standard deviations of the electron-pulse-height distributions obtained for heavy and light fragments, respectively. The variances of the means of these distributions for all of the odd record numbers were obtained from the expression

$$\sigma^2(\bar{\bar{\xi}}_{il}) = \sigma^2(\xi_i) / \sum_{w=1}^{m_1} n_{iw} , \tag{11c}$$

where $w = 1,3,5\ldots., m_1$. Similarly, the corresponding variances for all of the even record numbers were given by

$$\sigma^2(\bar{\bar{\xi}}_{i2}) = \sigma^2(\xi_i) / \sum_{w=2}^{m_2} n_{iw} , \tag{12C}$$

where $w = 2,4,6\ldots., m_2$. Finally, by propagation of the errors, the uncertainties associated with the average pulse heights and their ratio were obtained from the relations,

$$\sigma^2(<\bar{\xi}>_1) = [\sigma^2(\bar{\bar{\xi}}_{H1}) + \sigma^2(\bar{\bar{\xi}}_{L1})]/4 , \tag{13C}$$

$$\sigma^2(<\bar{\xi}>_2) = [\sigma^2(\bar{\bar{\xi}}_{H2}) + \sigma^2(\bar{\bar{\xi}}_{L2})]/4 , \tag{14C}$$

and

$$\sigma^2(R'_r)/(R'_r)^2 = \sigma^2(<\bar{\xi}>_1)/(<\bar{\xi}>_1)^2 + \sigma^2(<\bar{\xi}>_2)/(<\bar{\xi}>_2)^2 . \tag{15C}$$

The data obtained from the californium fragments were treated in a similar manner to obtain the values of ρ_r and $\sigma^2(\rho_r)$. In this case, however, the values of all the gammas were unity.

REFERENCES

1. N. Bohr, Nature 143, 330 (1939).
2. I. Halpern, Ann. Rev. Nucl. Sci. 9, 245 (1959).
3. D. Popovic, Proceedings of the International Conference on the Peaceful Uses of Atomic Energy, Geneva (United Nations, New York, 1955), Vol. 2, p. 164.
4. G. K. Green and L. W. Alvarez, Phys. Rev. 55, 417 (1939).
5. N. Feather, Nature 143, 597(1939).
6. R. R. Wilson, Phys. Rev. 72, 98 (1947).
7. O. Hahn and F. Strassmann, Naturwiss. 27, 11 (1939).
8. H. S. W. Massey and E. H. S. Burhop, Electronic and Ionic Impact Phenomena (Oxford University Press, New York, 1952), Chap. 9, Sec. 2, p. 541.
9. W. E. Stein and R. B. Leachman, Rev. Sci. Instr. 27, 1049 (1956).
10. J. S. Fraser and J. C. D. Milton, Nuclear Instr. 2, 275 (1958).
11. E. J. Sternglass, Phys. Rev. 108, 1 (1957).
12. N. Bohr, Kgl. Danske Videnskab, Selskab., Math. - fys. Medd. 18, No. 8 (1948), Chap. 3.
13. H. A. Bethe, Ann. Physik 5, 325 (1930).
14. A. J. Dekker, Solid State Physics, Vol. 6, (Academic Press, Inc., New York, 1958) p. 251.
15. C. Feldman, Phys. Rev. 117, 455 (1960).
16. P. H. J. A. Kleynen, Philips Tech. Rev. 2, 338 (1937).
17. D. J. Hughes, Pile Neutron Research (Addison-Wesley Publishing Co., Inc., Cambridge, Mass., 1953).

18. J. E. Evans, Fast Neutron Spectra from the Water Boiler, LA-1395 (1952).

19. H. de Waard, Nucleonics 13, No. 7, 36 (July 1955).

20. J. J. Katz and E. Rabinowitch, editors, Chemistry of Uranium, Part I, National Nuclear Energy Series VIII-5 (McGraw-Hill Book Co., Inc., New York, 1951) Chap. 12, p. 366.

21. T. S. Noggle and J. O. Stiegler, J. Appl. Phys. 31, 2199 (1960).

22. H. Bruining, Physics and Applications of Secondary Electron Emission (McGraw-Hill Book Co., Inc., New York, 1954) p. 42.

23. G. N. Walton, Progress in Nuclear Physics, Vol. 6 (Pergamon Press, New York, 1957) p. 192.

24. R. A. Schmitt, V. A. J. van Lint, and C. S. Suffredini, Third Symposium on Nuclear and Radiochemistry, Chalk River, September 1960.

25. The calibration data of Chapter IV were obtained with U-235 fragments originating from a fissile layer which was adjacent to the nickel foil. The expression required in the present calculation is the relative-electron-pulse height for other fragment types which originate not only from regions close to the nickel but also from positions throughout both the layer of thickness, L, and the nickel foil as well. Since the yield for nickel is only about 10 percent different from that of UF_4, as shown in Fig. 12, the error associated with the proximity of the nickel backing is expected to be negligible. The effective charges and velocities of the U-238 and Np-237 fragments which were used in this part of the experiment

are expected to differ slightly from those of the U-235 fragments. If this occurs, the absolute-electron-pulse heights will also be different from those obtained from the U-235 fragments. Even so, the relative-pulse height, H(x)/H(0), versus the depth, x, required here should be represented adequately by the empirical expression obtained in Chapter IV.

26. H. Bruining, loc. cit., p. 100.

27. J. E. Simmons and R. L. Henkel, Phys. Rev. 120, 198 (1960).

28. C. Eisenhart, M. W. Hastay, and W. A. Wallis, Selected Techniques of Statistical Analysis (McGraw-Hill Book Co., Inc., 1947) Chap. 2, p. 97.

29. D. B. Owen, Tables of Factors for One-Sided Tolerance Limits for a Normal Distribution, SCR-13 (1958).

30. R. Vandenbosch and J. R. Huizenga, Proceedings of the Second International Conference on the Peaceful Uses of Atomic Energy, Geneva (United Nations, New York, 1958), Vol. 15, Paper P/688.

31. Chromium Corporation of America, Waterbury, Connecticut.

32. Buckbee-Mears Company, Toni Building, St. Paul, Minnesota.

33. S. Bashkin and G. Goldhaber, Rev. Sci. Instr. 22, 112 (1951).

34. Y. Fujimoto and Y. Yamaguchi, Prog. of Theor. Phys. 5, 76 (1950).

IMPORTANT!

Special care should be taken to prevent loss or damage of this volume. If lost or damaged, it must be paid for at the current rate of typing.